

https://dspace.org/

Double-layer capacitance from the charged surface

Malaza, Nkosinathi

2016

http://hdl.handle.net/10539/21665

Malaza, Nkosinathi (2016) Double-layer capacitance from the charged surface, University of Witwatersrand, Johannesburg, <http://wiredspace.wits.ac.za/handle/10539/21665>

Downloaded from a DSpace repository. https://dspace.org/

University of the Witwatersrand

School of Physics

Master's Dissertation

Double-layer capacitance from the charged surface



STUDENT NAME:
Nkosinathi Malaza

STUDENT NUMBER:
320810

SUPERVISOR:
Prof. Alexander Quandt

CO-SUPERVISOR:
Dr. Robert Warmbier

A Dissertation submitted to the Faculty of Science, University of the Witwatersrand, Johannesburg, in fulfilment of the requirements for the degree of Master of Science.

28 October 2016

Declaration

I Nkosinathi Malaza, student number 320810 declare that this dissertation is as a result of my own work carried out at the University of the Witwatersrand.
It is not the same as any work that I have submitted, or is being concurrently submitted for a degree or other qualification at the University of the Witwatersrand or any other similar institution.
This work was carried out under the supervision of Prof. Alexander Quandt and Dr. Robert Warmbier.

Signature: 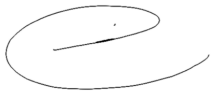

Name: Nkosinathi Malaza

Date: 28 October 2016

Place: University of the Witwatersrand, Johannesburg

Abstract

Energy storage has become an important issue for society, there is a need for affordable and efficient devices that can store energy optimally. Supercapacitors are energy storage devices that can solve society's energy storage problem. They can store the energy generated by renewable energy systems. In this work approaches will be studied that may be used to estimate capacitance of materials that can be used as the electrode of these devices. These materials must have high energy density, which will address one of the limitations of supercapacitors. To estimate the capacitance of the double layer, the double layer theory and ab initio numerical tools based on density functional theory (DFT) are used. The ab initio tools work with periodic systems, when charging the system one violates the periodicity of the system. This is overcome by using the effective screening medium method, which prevents energy divergent of the system. In this work different configurations of the water molecules are used to average the different orientations of water molecules in the electrolyte. The Pt(111) electrode is used, and electrolyte of sodium ion and water. In different configurations the sodium ion in the electrolyte is located at different positions. The capacitances calculated using two different approaches that we developed in this work are comparable to previously estimated capacitance. This is achieved by using minimal computational efforts. In previous studies the double layer capacitance was estimated to be in the range of 5 $\mu\mathrm{F}\cdot\mathrm{cm}^{-2}$ and 20 $\mu\mathrm{F}\cdot\mathrm{cm}^{-2}$, we obtained capacitance within that range. Double layer capacitance can be estimated to a good accuracy with the methods developed in this work. Though there are improvements that can be made on the methods that have been developed in this work to better estimate the double layer capacitance. And also more research has to be done in this field to come up with a theory that will accurately estimate capacitance. At the moment calculating the double layer capacitance is not trivial due to the lack of theory that describe the processes taking place at the surface of the electrode where the capacitance is calculated.

Dedicated to my lovely mother Nomoya Bhellina Malaza and my sister Lindiwe Mahlangu.

Acknowledgements

To my supervisors Prof. Alexander Quandt and Dr. Robert Warmbier, thank you for introducing me to scientific research. I appreciate your patience and support that you have given me.

And to materials for energy research group (MERG), thank you for giving me the funding to be able to carry out this work.

Contents

1 Double layer theory **9**
1.1 Electrical double layer 9

2 Density Functional Theory **16**
2.1 Introduction 16
2.2 Kohn-Hohenberg Theorems 16
2.3 Kohn-Sham density functional theory 19

3 Numerical details **23**
3.1 Periodic boundary conditions 23
3.2 Plane wave basis sets 23
3.3 Effective Screening Medium 26
3.4 Quantum Espresso 30

4 Results and discussion **31**
4.1 Preliminary results 31
4.2 Simulation of double layers 36
4.2.1 Charge on the system 37
4.2.2 Electrostatic potential 39
4.2.3 Dipole potential 40
4.2.4 Charge density 42
4.3 Capacitance 43
4.3.1 Capacitance from potential difference: 43
4.3.2 Capacitance from total energy difference: 45
4.4 Summary and Future work 47

5 Appendix **49**

Introduction

In this work capacitance will be studied theoretically and numerically by using the double layer theory at the interface between a metal electrode and an electrolyte.

Energy storage has been of great concern in the modern society considering the number of power outages we have been experiencing in South Africa. The energy that is generated by renewable energy systems needs to be stored and sustained to be able to use the energy whenever it is needed. These energy storage mechanisms need to be environmentally friendly, sustainable, easily accessible and affordable. At the moment the energy storage devices we are exposed to are primarily batteries, in particular lithium-ion batteries. Batteries have traditionally been used to power most electronic devices, including electric cars like the Tesla cars [1]. The Tesla model S car has a large lithium-ion battery that is used to store the energy to power the car [2]. Batteries store energy based on electrochemical reactions. Studies have been conducted on the performance of lithium-ion batteries during charging and discharging [3, 4]. It has been found that the charging and discharging of batteries are very slow and the life-time is short, but they are able to store large amounts of energy.

There is a need for devices that can perform better compared to batteries for energy storage. These devices should be able to store energy at a large scale that can be used by companies that provide electricity to the community. So these devices should have fast charging and discharging cycles, thus providing large energy release. Supercapacitors [5, 6, 7] are good candidates to improve the short term storage of energy. They are very efficient for energy storage under high power conditions. For example; electric vehicles store energy while braking and rapidly release energy during acceleration. Supercapacitors use different mechanisms of energy storage than batteries, as they primarily aim at improving the capacitance of an electrochemical device[8, 9]. Supercapacitors use high surface area electrodes and thin dielectric layers of ions and electrolyte to achieve a very high capacitance. Compared to other devices used in the electric cars for energy storage,

they perform much better [10]. This performance comparison is based on the energy storage efficiency, charging and discharging rates [11]. Especially in situations where large amounts of energy are needed like during acceleration of the vehicle. Energy recharge happens when the vehicle brakes, and they are much more responsive than batteries [12]. Supercapacitors can also be used as uninterrupted power supply (UPS). The UPS is an electrical device that is used to provide emergency power when there is a power surge or load shedding [13]. It provides power at an instant during a power cut, by supplying the energy that is stored in the supercapacitors in the UPS. The world's largest UPS is in Alaska, and it provides power to the Golden Valley Electric Association (GVEA). GVEA itself provides electricity to Fairbanks city in Alaska and the neighbouring communities when there is a power cut [14].

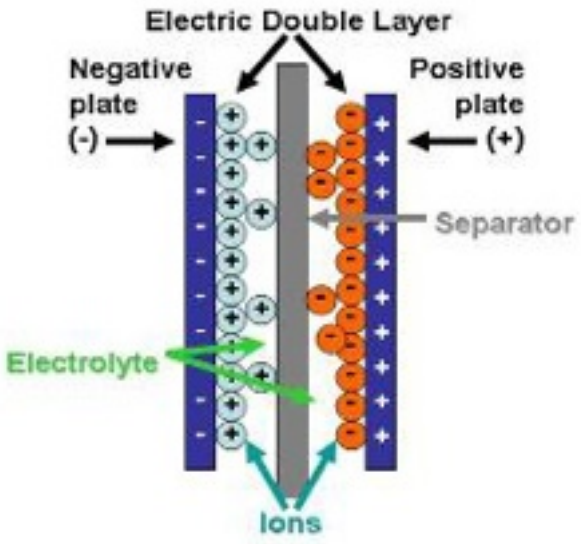

Figure 1: Schematic diagram for electric double layer capacitors (EDLCs) [15].

Supercapacitors can be classified according to their different types of energy storing mechanisms. Some mechanisms involve chemical reactions taking place, and there are other mechanisms were no chemical reactions take place during the energy storage process. The different types of supercapcitors are: pseudocapacitors, electric double layer capacitors, and hybrid capacitors. The mechanisms for energy storage involve the Faradaic process in pseudocapacitors, non-Faradaic process in electric double layer capacitors and a combination of both mechanisms in hybrid capacitors [11].

From henceforth in this work the electric double layer capacitors will be refereed using the acronym EDLCs, as they are popularly known.

EDLC devices are made up from two electrodes, a separator and an elec-

trolyte, as seen in Figure 1. The electrode is a metal or porous material where charges accumulate on the surface, thus creating a double layer with ions from the electrolyte [16]. The double layer will be discussed in the next chapter. The double layer formation will result in the storage of energy, the higher the surface area of the electrode the more energy will be stored. The capacitance is given by $C = \varepsilon A/d$, where A is the surface area of the electrode, ε is the dielectric constant of electrolyte and d is the thickness of the capacitor. This is the classical capacitance of a plate capacitor. The stored energy E is directly proportional to the capacitance C, $E = \frac{1}{2}CV^2$, where V is the electrostatic potential across the two electrodes. The separator is used to separate the two oppositely charged electrodes in order to avoid electric short-circuiting of the system. Studies have been conducted on various porous materials that can be used as the electrode for the double layer capacitance. These studies include activated carbons [17, 18]. They found that the activated carbons with larger pores are much suited for high power supercapacitance. However, there are also limitations on the storage of charges in the pores of the activated carbons [19]. The limitations include the stability of the material when exposed to charges. Other materials that are used as electrodes include aluminium, platinum and carbon materials. The double layer capacitance for carbon materials is estimated to be between 5 $\mu\mathrm{F}\cdot\mathrm{cm}^{-2}$ and 20 $\mu\mathrm{F}\cdot\mathrm{cm}^{-2}$ [20]. In literature the double layer capacitance for other electrode is estimated to be in the same range.

A model system of solid/electrolyte interface will be studied in this work and its capacitance will be calculated. Studies of charged solid/electrolyte interfaces have been active research since the days of Hermann von Helmholtz. So first, the concept of the double layer theory that was introduced by Helmholtz will be discussed. Second, the numerical details that are used to calculate the properties of the model system will be discussed, which will enable to calculate capacitance. The computational tools used in this work to study the double layer capacitance are based on ab initio methods. Finally, I will discuss results and give an outlook on future studies. Only a single electrode will be studied to calculate the capacitance of the system.

Chapter 1

Double layer theory

1.1 Electrical double layer

The double layer model was first introduced in the mid 1800s by Hermann von Helmholtz [21]. He showed that when one puts a charged electrode into an electrolyte solution, there will be a double layer formation at the interface. The charged electrode will not come into direct contact with ions of the same charge, due to electrostatics governed by Coulomb's law. But ions of different charge will be attracted to the surface of the electrode. Then a layer will form close to the electrode, made of ions surrounded by a shell of solvent molecules. This system is called a double layer. The Helmholtz model is useful in visualising the environment of ions near charged surfaces. These charged surfaces can be metals with applied potentials, or ions on the surface of an insulator. The chemical potential of the system is spatially dependent on x, the distance from the electrode. It is expressed as,

$$\mu(x) = zeV(x) + kT \ln \rho(x). \tag{1.1}$$

Where V is the electrostatic potential, $Q = ze$ is the total charge of the ion, $\rho(x)$ is the charge density of ions at a particular point x, k is the Boltzmann constant and T is the absolute temperature.

The total charge density is given by

$$\rho(x) = \sum_i n_i(x) z_i e, \tag{1.2}$$

when one sums over all ions in the system, and $n_i(x)$ is the concentration of these ions in the electrolyte.

This model was further studied by Louis Gouy in 1910 [23], he was the first to consider the charged ions of the electrolyte in spatial distribution. He took

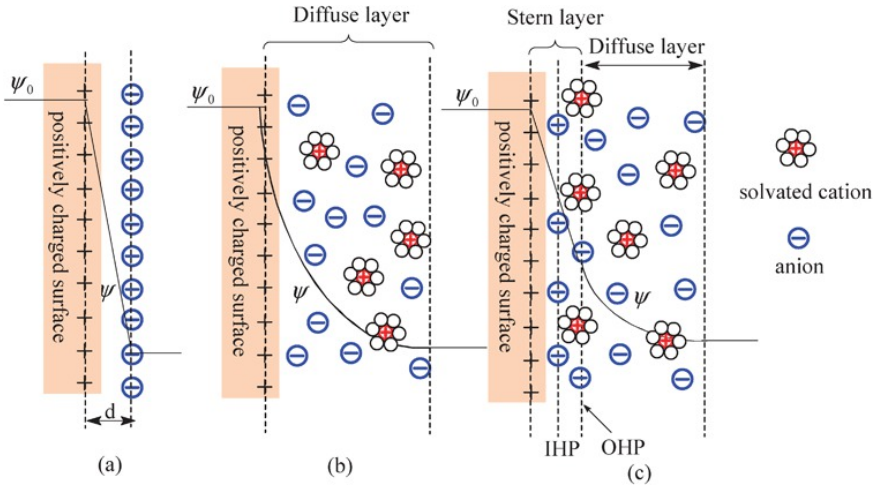

Figure 1.1: [22] The potential is represented as ψ, which is the same as the electrostatic potential V, i.e. $\psi \equiv V$. The double-layer models that were studied by: (a) Helmholtz, (b) Gouy and Chapman, (c) Stern with the inner Helmholtz plane(IHP) and outer Helmholtz plane (OHP).

into account that these ions will be subjected to electric fields. In 1913 David Chapman [24] used Poisson equation to describe this situation assuming that the interface has no dipoles. This implies that the potential is uniform, i.e. the inner potential is the same as the outer potential. For a charged system to be in equilibrium the potential must be uniform throughout the surface. This keeps the overall charge on the double layer neutral. From Figure 1.1, we can see that at $x = 0$, which is on the surface of the electrode, the electric potential is zero, $V_0 = 0$. Combining this with equation (1.1) we obtain the chemical potential of ions on the surface,

$$\mu(0) = zeV_0 + kT \ln \rho_0, \tag{1.3}$$

where ρ_0 is the concentration of ions at the surface of the electrode [25].

With $V_0 = 0$, we get

$$\mu(0) = kT \ln \rho_0 \tag{1.4}$$

From equation (1.1), suppose that μ is the same throughout the system, i.e. the system is in equilibrium, we find that $\mu(0) = \mu(x)$. This gives,

$$kT \ln \rho_0 = zeV(x) + kT \ln \rho(x). \tag{1.5}$$

By summing over all ionic species in the electrolyte, we get a slightly different equation

$$kT \ln \rho_0 = \sum_i z_i eV(x) + kT \ln \rho(x). \tag{1.6}$$

Which leads to,

$$\ln\left(\frac{\rho(x)}{\rho_0}\right) = \sum_i -\frac{z_i e V(x)}{kT}. \tag{1.7}$$

From equation (1.7) follows the expression for the charge density $\rho(x)$

$$\rho(x) = \rho_0 \sum_i \exp\left[-\frac{z_i e V(x)}{kT}\right], \tag{1.8}$$

which is a Boltzmann distribution.

Chapman observed that the excess charge density ρ as a function of distance x, from the surface can be expressed by the Poisson equation.

$$\rho(x) = -\varepsilon\varepsilon_0\left(\frac{d^2V(x)}{dx^2}\right), \tag{1.9}$$

where ε is the dielectric constant of the electrolyte and ε_0 is the permittivity of free space.

The Helmholtz model itself does not consider the dependence of capacitance on the applied potential. Gouy-Chapman observed that an applied potential increases the concentration of ions near the electrode, and the capacitance will also change. They developed a double-layer model that operates with diffusion of ions between different interfaces. In this diffusion model of the double layer, the Maxwell-Boltzmann statistics [26] can be applied, where the ions are distributed as a function of their distance from the electrode surface. This results in an exponential decrease of the electric potential away from the surface. In recent years a lot of research has been made to validate the Gouy-Chapman model. In one of the studies the authors modelled an interface of a metal with ionic liquid solution [27], and they predicted the capacitance of that system as a function of the applied potential.

Otto Stern in 1924 [28] investigated the Helmholtz double layer model again in order to improve the Gouy-Chapman model; in cases when a strong potential is applied to charge the surfaces of the electrodes. Stern basically combined the two models, the Helmholtz and Gouy-Chapman model: One of the assumptions that Gouy-Chapman made is that the ions can be regarded as point charges [29], and that ions can get close to the surface. This assumption is not physically valid, as the ions are surrounded by solvent molecules. Ions themselves have finite size, they are not point charges [30], and therefore they cannot directly be in contact with the surface of the electrode [31]. Stern postulated a so-called Stern layer, which consists of the inner Helmholtz plane (IHP) and the outer Helmholtz plane (OHP). In the

inner Helmholtz plane the ions are strongly adsorbed on the surface of the electrode, while on the outer Helmholtz plane the ions are not specifically adsorbed. Beyond the outer Helmholtz plane a diffuse layer is formed.

Using the above assumptions one can derive expressions for the capacitance of the system. By combining equation (1.8) and (1.9) we get,

$$\frac{d^2V(x)}{dx^2} = -\frac{\rho_0}{\varepsilon\varepsilon_0}\sum_i \exp\left[\frac{-z_i eV(x)}{kT}\right]. \tag{1.10}$$

For simplicity I will drop the explicit x dependence of V in the following. Using the relation,

$$\frac{d^2V}{dx^2} = \frac{1}{2}\frac{d}{dV}\left(\frac{dV}{dx}\right)^2, \tag{1.11}$$

equation (1.10) can be expanded as,

$$d\left(\frac{dV}{dx}\right)^2 = -\frac{2}{\varepsilon\varepsilon_0}\rho_0\sum_i \exp\left(-\frac{z_i eV}{kT}\right)dV. \tag{1.12}$$

Furthermore, one can use the definition of the charge density in equation (1.2) to replace ρ_0:

$$d\left(\frac{dV}{dx}\right)^2 = -\frac{2}{\varepsilon\varepsilon_0}\sum_i n_i z_i e\exp\left(-\frac{z_i eV}{kT}\right)dV. \tag{1.13}$$

Equation (1.13) is now in an integrable form, and we get

$$\left(\frac{dV}{dx}\right)^2 = \frac{2kT}{\varepsilon\varepsilon_0}\sum_i n_i\left[\exp\left(-\frac{z_i V}{kT}\right) + C\right], \tag{1.14}$$

where n_i is the ion concentration in the bulk, and C is an integration constant. To determine this constant we consider the ions far away from the electrode, where the system is neutral, and so we have the condition $V = 0$. This condition can be formally expressed as,

$$\lim_{x\to\infty} V(x) = 0. \tag{1.15}$$

From Figure 1.1, it can be observed that far away from the surface the electric potential V becomes constant. This will result in $\left.\frac{dV}{dx}\right|_{x\to\infty} = 0$, and with the condition in equation (1.15) implies that $C = -1$, and

$$\left(\frac{dV}{dx}\right)^2 = \frac{2kT}{\varepsilon\varepsilon_0}\sum_i n_i\left[\exp\left(-\frac{z_i eV}{kT}\right) - 1\right]. \tag{1.16}$$

Finally, let us consider a system with symmetric electrolyte. This means that the electrolyte has only one cationic species and one anionic species both with the same charges of different sign. This mean that $|z_+| = |z_-| = z$ and $n_+ = n_- = n$, so we can drop the summation above. Then equation (1.16) is written as,

$$\left(\frac{dV}{dx}\right)^2 = \frac{2kTn}{\varepsilon\varepsilon_0}\left[\exp\left(-\frac{zeV}{kT}\right) - 1 + \exp\left(\frac{zeV}{kT}\right) - 1\right]. \tag{1.17}$$

In this work we study a system with a negatively charged electrode, this further simplifies equation (1.17). Then we can write the equation as,

$$\frac{dV}{dx} = \sqrt{\frac{8kTn}{\varepsilon\varepsilon_0}}\sinh\left(\frac{zeV}{2kT}\right). \tag{1.18}$$

A detailed derivation from equation (1.17) to equation (1.18) is given in the Appendix (i). The surface charge density, being the charge per unit area of the electrode, is given by

$$\sigma = \varepsilon\varepsilon_0\left(\frac{dV}{dx}\right)\Big|_{x=0}. \tag{1.19}$$

The potential difference between the surface and the outer Helmholtz plane(OHP) is given by,

$$\frac{dV}{dx} = \frac{V_d - V_0}{d}, \tag{1.20}$$

where d is the thickness of the Helmholtz layer as seen in Figure 1.1, V_0 and V_d are potential on the surface of the electrode and in the Helmholtz layer respectively.

Then,

$$V_0 = V_d - \frac{\sigma}{\varepsilon\varepsilon_0}d. \tag{1.21}$$

Substitute equation (1.19) and (1.21) into equation (1.18), to get:

$$\sigma = \sqrt{8kTn\varepsilon\varepsilon_0}\sinh\left[\frac{ze\left(V_d - \frac{\sigma}{\varepsilon\varepsilon_0}d\right)}{2kT}\right]. \tag{1.22}$$

Capacitance is defined as the ratio of the change in surface charge density with respect to the change in potential,

$$C = \frac{d\sigma}{dV}. \tag{1.23}$$

Taking the inverse of equation (1.23) will make it easier to calculate the capacitance.

In equation (1.22), let $A = \sqrt{8kTn\varepsilon\varepsilon_0}$, $B = \frac{ze}{2kT}$, $D = \frac{zed}{2kT\varepsilon\varepsilon_0}$

Then equation (1.22) becomes,

$$\sigma = A\text{sinh}\,(BV_d - D\sigma). \tag{1.24}$$

Rearranging equation (1.24) and taking the inverse of the hyperbolic sine, we get:

$$V_d = \frac{\text{arsinh}\left(\frac{\sigma}{A}\right)}{B} + \frac{D\sigma}{B}. \tag{1.25}$$

The inverse of the expression of capacitance in equation (1.23) is,

$$\frac{1}{C} = \frac{dV}{d\sigma}. \tag{1.26}$$

Taking the derivative of equation (1.25) and using the derivative of the hyperbolic sine, to get

$$\frac{1}{C} = \frac{1}{AB}\frac{1}{\sqrt{\left(\frac{\sigma}{A}\right)^2 + 1}} + \frac{D}{B}. \tag{1.27}$$

Substituting back A, B and D and simplifying equation (1.26),

$$\frac{1}{C} = \frac{d}{\varepsilon\varepsilon_0} + \frac{2kT}{ze\left[\sigma^2 + 8kT\varepsilon\varepsilon_0 n\right]^{\frac{1}{2}}}. \tag{1.28}$$

This is the total capacitance of the system, the sum of capacitance of Helmholtz layer and diffuse layer. The first term is the Helmholtz capacitance and the second term is diffuse layer capacitance. The above equation can be written as

$$\frac{1}{C} = \frac{1}{C_H} + \frac{1}{C_d}. \tag{1.29}$$

In this work only the Helmholtz capacitance will be studied,

$$C = \frac{\varepsilon\varepsilon_0}{d} \tag{1.30}$$

$$= \frac{\sigma}{\Delta V}. \tag{1.31}$$

This expression for capacitance is the same as the expression for capacitance of parallel plates with a medium of dielectric constant ε. To calculate

the capacitance of the double layer, one need to know the surface charge density and the potential difference. The derivation for the expression of capacitance above can also be obtained in electrochemistry textbooks [32, 33]. To get these quantities computational tools will be used to assist in simulating double layer and obtain the required information. These tools use density functional theory, which will be discussed in the next chapter.

Chapter 2

Density Functional Theory

2.1 Introduction

This is a brief discussion of the modelling methods that are mostly utilised to investigate the ground state properties of the systems of interest. Density Functional Theory(DFT)[34, 35, 36] is used to investigate the ground state properties of a given system. It is a theory where one replaces the many-body wave functions with an electron density $\rho(\vec{r})$ as basic physical entity. Note that for a system of N electrons the wave function depends on three spatial variables, $3N$. It is then much easier to use the electron density, which depends on only 3 spatial variables. Therefore DFT can be applied to larger systems with hundreds of atoms. The DFT formalism also simplifies numerical ab initio computations for many-electron systems, and in particular for solids. DFT is based on two famous theorems by Hohenberg and Kohn [37], and its practical implementation goes back to Kohn and Sham [38].

2.2 Kohn-Hohenberg Theorems

To investigate the properties of a many-electron system Hohenberg and Kohn established two famous theorems [37] .

They assumed that the electronic structure of matter may be explained using the time independent Schrödinger equation. For an N-electron system, the Schrödinger equation is given by

$$\hat{H}\Psi = E\Psi. \tag{2.1}$$

Where $\hat{H}$ is the many-electron Hamiltonian operator, Ψ is the wave function and the total electronic energy related to Ψ is E.

The Hamiltonian is given by

$$\hat{H} = \sum_{i}^{N} \left(-\frac{1}{2}\nabla_i^2 \right) + \sum_{i}^{N} \upsilon(\vec{r}_i) + \sum_{i<j}^{N} \frac{1}{r_{ij}}, \tag{2.2}$$

where $\upsilon(\vec{r}_i) = \sum_\nu \frac{Z_\nu}{r_{i\nu}}$ is the external potential acting on electron i which is caused by nuclear charges Z_ν. Atomic units are assumed, $\hbar = m = e^2 = 1$.

The ground state energy and the wave function are determined by minimizing the energy functional,

$$E[\Psi] = \frac{\left\langle \Psi | \hat{H} | \Psi \right\rangle}{\langle \Psi | \Psi \rangle}. \tag{2.3}$$

Here the expectation values of the Hamiltonian operator is given by:

$$\left\langle \Psi | \hat{H} | \Psi \right\rangle = \int d\vec{x} \Psi^* \hat{H} \Psi. \tag{2.4}$$

For arbitrary Ψ we find that,

$$E[\Psi] \geq E_0 \tag{2.5}$$

This equation tells us that the total energy functional related to a general wave function Ψ, is greater than the ground state energy E_0. By minimizing $E[\Psi]$ over all possible wave functions, only the wave function related to the ground state energy E_0 will minimize $E[\Psi]$,

$$E_0 = \overset{min}{\Psi} E[\Psi]. \tag{2.6}$$

In 1964 Kohn and Hohenberg [37], proposed their first theorem, which states that the external potential $\upsilon(\vec{r})$ is in one-to-one correspondence to the ground state electron density $\rho(\vec{r})$.

The ground state energy is assumed to be a functional of the ground state electron density, $\rho(\vec{r})$, i.e.

$$E = E[\rho]. \tag{2.7}$$

To prove this theorem one would consider two N-electron systems with different external potentials $\upsilon_1(\vec{r})$ and $\upsilon_2(\vec{r})$. Each of these potentials is supposed to give the same electron density ρ in the ground state. With two different external potentials we would however have two Hamiltonians H_1 and H_2 with different eigenstates Ψ_1 and Ψ_2 but the same ground state density.

Using the variational principle of equation (2.5) and taking Ψ_1 as a trial function for the Hamiltonian H_2, we find that

$$E_1 < \langle \Psi_2 | H_1 | \Psi_1 \rangle = \langle \Psi_2 | H_2 | \Psi_2 \rangle + \langle \Psi_1 | H_1 - H_2 | \Psi_1 \rangle \tag{2.8}$$

$$= E_2 + \int \left[\upsilon_1(\vec{r}) - \upsilon_2(\vec{r}) \right] \rho(\vec{r}) d\vec{r}, \tag{2.9}$$

where E_1 and E_2 are the ground state energies for H_1 and H_2, respectively. Similarly, taking Ψ_2 as the trial wave function for the Hamiltonian H_1,

$$E_2 < E_1 + \int \left[\upsilon_2(\vec{r}) - \upsilon_1(\vec{r}) \right] \rho(\vec{r}) d\vec{r}. \tag{2.10}$$

Then adding equation (2.9) and (2.10), gives

$$E_1 + E_2 < E_2 + E_1 \tag{2.11}$$

This is a contradiction! One would conclude that the two N-electron Hamiltonians which differ by their external potentials cannot give the same ground state density, ρ. This proves the first theorem, and shows that ρ uniquely determines the external potential υ, the N-electron Hamiltonian, and all ground state properties related to ρ.

One can express the total energy $E[\rho]$ depending on the electron density $\rho(\vec{r})$ for a given external potential $\upsilon(\vec{r})$ as:

$$E_\upsilon[\rho] = T[\rho] + V_{ne}[\rho] + V_{ee}[\rho]. \tag{2.12}$$

Where $T[\rho]$ is the ground state kinetic energy functional, $V_{ne}[\rho]$ is the electron-nucleus attraction functional, and $V_{ee}[\rho]$ is the electron-electron repulsion functional.

$$E_\upsilon[\rho] = \left\langle \Psi[\rho] | \hat{T} + \hat{V}_{ee} + \hat{V}_{ne} | \Psi[\rho] \right\rangle \tag{2.13}$$

$$= \left\langle \Psi[\rho] | \hat{T} + \hat{V}_{ee} | \Psi[\rho] \right\rangle + \int d\vec{r} \upsilon(\vec{r}) \rho(\vec{r}). \tag{2.14}$$

This can be written as,

$$E_\upsilon[\rho] = F[\rho] + \int \upsilon(\vec{r}) \rho(\vec{r}) d\vec{r}. \tag{2.15}$$

Where $F[\rho]$ is a universal functional, which is independent of the external potential and only depends on the electron density $\rho(\vec{r})$. The minimum value of $E_\upsilon[\rho]$ is the ground state energy E_0.

The second theorem states that: When $E[\rho]$ is varied over the allowed class of trial densities then the minimum value is the true ground state energy, and the related density $\rho_0(\vec{r})$ is the true ground state density. This is given as,

$$E_\upsilon[\rho] \geq E_0[\rho_0]. \tag{2.16}$$

A proof of this theorem can be found in [39].

2.3 Kohn-Sham density functional theory

The many-electron ground state energy is obtained by minimizing the energy functional in equation (2.15) [39, 36]. The corresponding electron density ρ, satisfies the Euler-Lagrange equation

$$\frac{F[\rho]}{\delta\rho(\vec{r})} + \upsilon(\vec{r}) - \mu = 0, \tag{2.17}$$

where μ is the chemical potential. Which means that $E_\upsilon[\rho]$ is minimized under the constraint

$$N = \int \rho(\vec{r})d\vec{r}, \tag{2.18}$$

and μ is the corresponding Lagrangian multiplier.

The solutions of equation (2.17) should minimize $E[\rho]$, but to determine $F[\rho]$ we need to approximate $T[\rho]$ and $V_{ee}[\rho]$. Thomas-Fermi and other models contain direct approaches to approximate these quantities [39]. These approaches are simple, but they have their limitations, and thus compromise the accuracy of the approximation for $T[\rho]$ and $V_{ee}[\rho]$.

Kohn and Sham [38] postulated an indirect approach that trades simplicity for accuracy of the approximation. Kohn-Sham realised that the failure of the Thomas-Fermi model was due to the poor description of the kinetic energy. To overcome this problem, they developed an orbital theory based on a non-interacting reference system with mean field potential υ_s.

Then the electron density of this non-interacting reference system is given by,

$$\rho(\vec{r}) = \sum_{i=1}^{N} |\psi_i|^2, \tag{2.19}$$

where ψ are Kohn-Sham orbitals.

For the reference system Kohn-Sham postulated a general single electron Hamilton operator,

$$\hat{h}_s = \sum_i^N \left(-\frac{1}{2}\nabla_i^2 + \upsilon_{eff}(\vec{r_i}) \right). \tag{2.20}$$

The corresponding Schrödinger equation is given by,

$$\hat{h}_s\psi_i = \left[-\frac{1}{2}\nabla^2 + \upsilon_{eff}(\vec{r}) \right] \psi_i = \varepsilon_i\psi_i. \tag{2.21}$$

The electrons interact only via the mean field potential, υ_{eff}. One may use a Slater determinant to determine the ground state wave function for the full non-interacting N-electron system,

$$\Psi_s = \frac{1}{\sqrt{N!}} det\left[\psi_1\psi_2\psi_3...\psi_N\right]. \tag{2.22}$$

The kinetic energy of this non-interacting reference system is,

$$T_s[\rho] = \left\langle \Psi_s \left| \sum_{i=1}^N \left(-\frac{1}{2}\nabla_i^2 \right) \right| \Psi_s \right\rangle. \tag{2.23}$$

With this wave function, we can approximate the kinetic energy in equation (2.23). However $T_s[\rho]$ is not the same as the kinetic energy function in the universal functional $F[\rho]$. To overcome this, Kohn-Sham re-wrote equation (2.15) by writing it as a sum of the kinetic energy of the non-interacting reference system T_s, the electron-electron repulsion potential V_{ee}, and the exchange correlation energy E^{xc}.

$$F[\rho] = T_s[\rho] + V_{ee}[\rho] + E^{xc}[\rho]. \tag{2.24}$$

The exchange correlation energy then includes all the quantum effects of the system, which are correlations and corrections of the approximate kinetic energy T_s.

Then the total energy in equation (2.15) is given by,

$$E[\rho] = T_s[\rho] + V_{ee}[\rho] + E^{xc}[\rho] + \int \upsilon(\vec{r})\rho(\vec{r})d\vec{r}. \tag{2.25}$$

To get the Kohn-Sham effective potential υ_{eff} from equation (2.25),

$$\upsilon_{eff} = \frac{\delta E[\rho]}{\delta\rho(\vec{r})} = \frac{\delta\left\{T_s[\rho] + V_{ee}[\rho] + E^{xc}[\rho] + \int \upsilon(\vec{r})\rho(\vec{r})d\vec{r}\right\}}{\delta\rho(\vec{r})} \tag{2.26}$$

The kinetic energy functional of the non-interacting reference system $T_s[\rho]$, and the electron-electron repulsion potential V_{ee} are part of the exchange correlation functional $E^{xc}[\rho]$ from equation (2.24). Then equation (2.26) can be written as,

$$\upsilon_{eff} = \frac{\delta E^{xc}[\rho]}{\delta\rho(\vec{r})} + \upsilon(\vec{r}) + \int \frac{\rho(\vec{r}')}{|\vec{r} - \vec{r}'|} d\vec{r}'. \tag{2.27}$$

Where, the first term is the exchange correlation potential

$$\upsilon^{xc}(\vec{r}) = \frac{\delta E^{xc}[\rho]}{\delta\rho(\vec{r})}. \tag{2.28}$$

The second term is the external potential, $\upsilon(\vec{r})$, and the third term is the classical Coulomb potential,

$$\upsilon_C = \int \frac{\rho(\vec{r}')}{|\vec{r} - \vec{r}'|} d\vec{r}'. \tag{2.29}$$

The classical Coulomb potential includes the electron-electron repulsion potential.

Then equation (2.27) can be written as,

$$\upsilon_{eff} = \upsilon^{xc}(\vec{r}) + \upsilon(\vec{r}) + \upsilon_C. \tag{2.30}$$

If we now vary $E_\upsilon[\rho]$ under the constraint of orthonormal ψ_i,

$$\varepsilon_i\psi_i = \left[-\frac{1}{2}\nabla^2 + \upsilon_{eff}(\vec{r})\right]\psi_i. \tag{2.31}$$

This equation explains that the motion of the electrons of an interacting system can be mapped on a non-interacting system as suggested in equation (2.21); where electrons are considered to be moving in a mean field potential called the effective potential. The complicated interactions of the electrons are all contained in this effective potential υ_{eff}.

The total energy according to Kohn-Sham is given by,

$$E = \sum_i^N \varepsilon_i - \frac{1}{2}\int\int \frac{\rho(\vec{r}')\rho(\vec{r})}{|\vec{r} - \vec{r}'|} d\vec{r}' d\vec{r} + E^{xc}[\rho] - \int \upsilon^{xc}(\vec{r})\rho(\vec{r}) d\vec{r}, \tag{2.32}$$

where,

$$\sum_i^N \varepsilon_i = \sum_i^N \left\langle \psi_i \left| -\frac{1}{2}\nabla^2 + \upsilon_{eff}(\vec{r}) \right| \psi_i \right\rangle \tag{2.33}$$

$$= T_s[\rho] + \int \upsilon_{eff}(\vec{r})\rho(\vec{r}) d\vec{r}. \tag{2.34}$$

Then substituting equation (2.34) into the total energy in equation (2.32), we get

$$E = T_s[\rho] + E^{xc}[\rho] + \int \upsilon_{eff}(\vec{r})\rho(\vec{r})d\vec{r} - \frac{1}{2}\int\int \frac{\rho(\vec{r}')\rho(\vec{r})}{|\vec{r}-\vec{r}'|}d\vec{r}'d\vec{r} - \int \upsilon^{xc}(\vec{r})\rho(\vec{r})d\vec{r}. \tag{2.35}$$

Equations (2.19), (2.30), (2.31) and (2.35) are the Kohn-Sham equations. The Kohn-Sham effective potential υ_{eff} depends on the electron density $\rho(\vec{r})$ via equations (2.19) and (2.31). So in order to solve the Kohn-Sham equations, one must apply a self-consistent method. This is done by starting from an initial guess of $\rho(\vec{r})$, then construct the effective potential using equation (2.30) and obtain the Kohn-Sham orbitals from the eigenvalue problem in (2.31). With these orbitals, we can calculate a new electron density $\rho(\vec{r})$ using equation (2.19). This process is repeated until convergence is achieved, and using the final electron density in equation (2.35) one may calculate the total energy $E_\upsilon[\rho]$ with respect to ρ.

The exchange correlation energy functional $E^{xc}[\rho]$ is generally unknown. It has to be approximated to get the total energy of the system. This allows for the improvement of the Kohn-Sham approach based on better approximations of the $E^{xc}[\rho]$. These equations also require less computational effort compared to similar theories, like the Hartree-Fock method [39]. A large variety of functionals have been suggested to approximate the exchange correlation functional. Recently, Perdew proposed a way to categorize these approximate functionals, which is called the Jacob's ladder [40]. For large systems the Kohn-Sham approach works better than the quantum chemistry methods [41], which are restricted to systems of 10 or less atoms. If the exchange correlation functional could ever be accurately approximated, it would give us the exact electron density $\rho(\vec{r})$ and the total ground state energy E.

Chapter 3

Numerical details

3.1 Periodic boundary conditions

There are different boundary conditions that can be imposed on a many-electron system.

There are systems without clear boundaries. This condition is called free boundary condition. It is applied to systems like molecules in vacuum. Extremely fast processes where the effects of boundary are negligible are also described by free boundary condition.

For rigid boundaries, some atoms at the boundaries are fixed. Such a configuration is not physical, and it has the serious disadvantage that it can induce artifacts. However this condition can often be combined with other and better boundary conditions.

In this work periodic boundary conditions is used. With periodic boundary conditions the fundamental simulation box is reduced to a unit cell. The atoms are contained within the unit cell, and the unit cell is repeated with no overlaps or any voids. All the unit cells have the same size, shape, and number of atoms in them. Equivalent atoms in the unit cells have the same positions and momentum. Atoms on the edges of the unit cell can interact with the copy-atom in neighbouring unit cells. So periodic boundary conditions help to create a structure similar to bulk solids.

3.2 Plane wave basis sets

In this work we only working with systems that are subjected to periodic boundary conditions. The nuclei of the electrons are arranged in a pattern that is repeating itself periodically. The effective potential that acts on the electrons is also periodic, i.e. $v_{eff}(\vec{r}) = v_{eff}(\vec{r}+\vec{R})$ with $\vec{r}$ being the position

of the electrons in the unit cell, and $\vec{R}$ being the lattice vector. The obvious choice of basis functions to study periodic systems are plane waves because of Bloch's theorem [42]. In Bloch's theorem a wave function ψ in a periodic potential $\upsilon_{eff}(\vec{r})$ takes the form,

$$\psi_k(\vec{r}) = e^{i\vec{k}\cdot\vec{r}} u_k(\vec{r}) \tag{3.1}$$

where $\vec{k}$ is the wave vector and $u_k(\vec{r})$ is a periodic amplitude function, i.e. $u_k(\vec{r}) = u_k(\vec{r}+\vec{R})$ with the same periodicity as the crystal structure. Equation (3.1) is a modulated plane wave, which is the product of a periodic function times a plane wave. Bloch states are not periodic, they take up a phase factor $e^{i\vec{k}\cdot\vec{R}}$ after translation by $\vec{R}$ as,

$$\psi_k(\vec{r}+\vec{R}) = e^{i\vec{k}\cdot(\vec{r}+\vec{R})} u_k(\vec{r}+\vec{R}) \tag{3.2}$$

$$\tag{3.3}$$

$$= e^{i\vec{k}\cdot\vec{R}} e^{i\vec{k}\cdot\vec{r}} u_k(\vec{r}) \tag{3.4}$$

$$= e^{i\vec{k}\cdot\vec{R}} \psi_k(\vec{r}) \tag{3.5}$$

Since the amplitude function $u_k(\vec{r})$ has the same periodicity as the crystal, one can expand it as follows:

$$u_k(\vec{r}) = \sum_{\vec{G}} c_{k,\vec{G}} e^{i\vec{G}\cdot\vec{r}} \tag{3.6}$$

where $\vec{G}$ is the reciprocal lattice vector from the so-called reciprocal space (or k-space). $\vec{G}$ is related to a Bravais lattice vector, $\vec{R}$ in real space by $\vec{G}\cdot\vec{R} = 2\pi n$ with $n \in \mathbb{Z}$ [42].

The Bloch state, equation (3.1) can now be written as:

$$\psi_k(\vec{r}) = \sum_{\vec{G}} c_{k,\vec{G}} e^{i(\vec{k}+\vec{G})\cdot\vec{r}} \tag{3.7}$$

The higher Fourier components $|\vec{G}+\vec{k}|$ have small contribution to equation (3.7) as they correspond to states with large kinetic energies. So cutting the expansion of the Bloch states at some values of $|\vec{G}+\vec{k}|$ defines the cut-off energy E_{cut}, with

$$\frac{\hbar^2|\vec{G}+\vec{k}|^2}{2m} \leq E_{cut}. \tag{3.8}$$

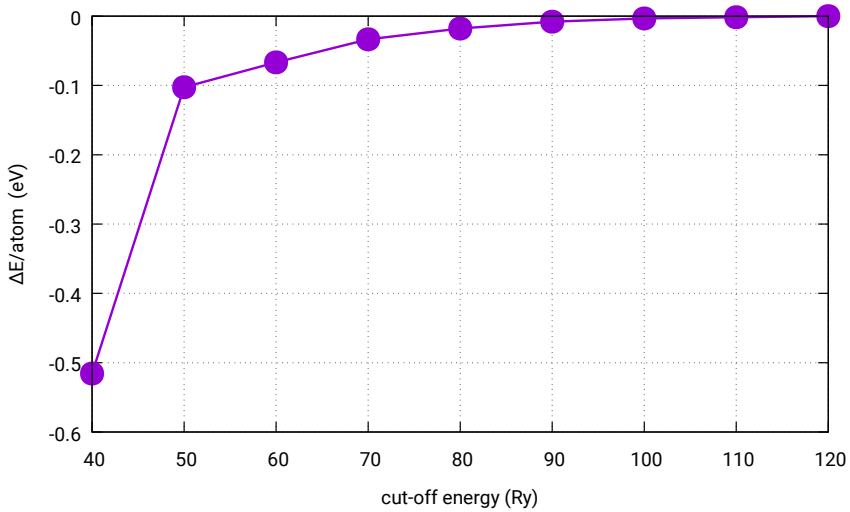

Figure 3.1: Cut-off energy convergence for PtH_2ONa system. The system consist of 27 platinum atoms, 32 water molecules and a sodium ion.

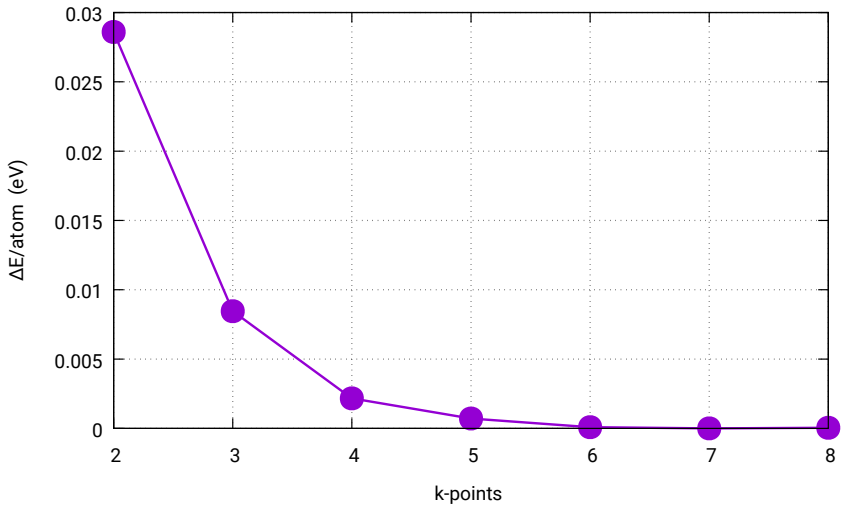

Figure 3.2: k-points convergence for PtH_2ONa system. The system consist of 27 platinum atoms, 32 water molecules and a sodium ion.

Rather than choosing all k-points within the first Brillouin zone to determine the Bloch states at these points, one only chooses a specific number of k-points, as implemented in the Monkhorst-Pack grid [43]. The grid is uniformly spaced at the points $nk1 \times nk2 \times nk3$ in the first Brilloiun zone. It is essential to converge all numerical results with respect to this reduced k-point grid and with respect to the cut-off energy E_{cut}. In this study we

converged the k-points and the cut-off energy for PtH_2ONa system. The system has 27 platinum atoms, 32 water molecules and a sodium ion. The results are shown in Figure 3.1 and 3.2, where the total energy difference per atom was plotted against the cut-off energy and k-points respectively. The cut-off energy I chose to use in this work is 60 Ry and the k-point grid is $(3 \times 3 \times 1)$. Denser k-point grids and larger basis sets will take longer to compute, and the given parameters are well within the converged range of parameters.

We effectively solve the single electron Schrödinger equation given in equation (2.31) for a solid, with a periodic effective Kohn-Sham potential v_{eff}, given in equation (2.30). The Kohn-Sham wave function ψ_i are Bloch states, which can be expanded using a plane wave basis sets like in equation (3.7). And the advantage of the plane-wave basis sets is the usage of the fast Fourier transformation(FFT) to calculate the electron density, external potential and the total energy [44, 45] .

3.3 Effective Screening Medium

The effective screening medium (ESM) approach [46], is a first principles computational method for charged systems. It was developed to overcome problems that one faces when trying to simulate a periodic repeated system with an applied electric potential. In such a system, the periodic boundary conditions are violated [47]. The ESM method solves this problem by removing periodic boundary conditions along a direction perpendicular to an electrode surface, but retaining periodicity parallel to the surface of an electrode. The slab is the interface between Pt and the ionic solution, and it is centred around zero. It is sandwiched between two media, which can be a vacuum, metal or dielectrics with respective relative dielectric constant $\epsilon(\vec{r})$. These media are referred to as the ESM. The electrons are restricted into the region between the two media with $x \in [-L/2, L/2]$. From Figure 3.3, the space w between the boundary of the cell and the ESM medium is vacuum, which is optional, and the size of the super cell is L in the z-direction. In Figure 3.3 the slab contains interfaces between an electrode and the electrolyte, and it is then shifted to the left or right of the unit cell so that it is centred around zero.

Introducing a potential $V(\vec{r})$ to the system as part of the ESM changes the Kohn-Sham total energy functional in equation (2.35) [46], becomes

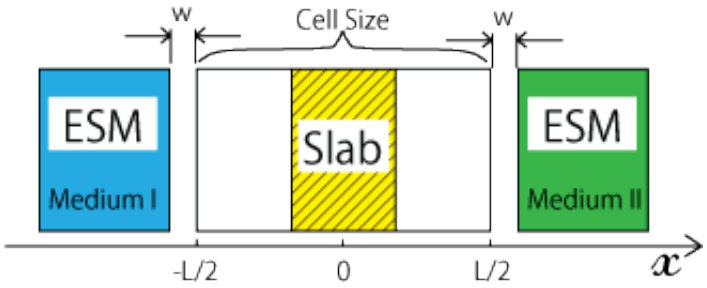

Figure 3.3: ESM scenario for double layer capacitance. Medium I and II can be a vacuum and/or metal, or it can be a dielectric. In this work, medium I and II are vacuum and/or metal. The width w, is the space between the boundary of the cell and the ESM medium. In this work the super cell lies along the z-direction, [48].

$$E[\rho_e, V] = T_s[\rho_e] + E_{ex}[\rho_e] + \int \frac{\epsilon(\vec{r})}{8\pi} |\nabla V(\vec{r})|^2 \, d\vec{r} + \int \left[\rho_e(\vec{r}) + \rho_c(\vec{r}) + \rho_n(\vec{r})\right] V(\vec{r}) d\vec{r}. \tag{3.9}$$

Here $\rho_e(\vec{r})$ is the electron charge density, $\rho_n(\vec{r})$ is the nuclear charge density and $\rho_c(\vec{r})$ is the classical charge density, which includes external charges. Then the total charge density is given by

$$\rho_t = \rho_e(\vec{r}) + \rho_n(\vec{r}) + \rho_c(\vec{r}). \tag{3.10}$$

And we can re-write equation (3.9),

$$E[\rho_e, V] = T_s[\rho_e] + E_{ex}[\rho_e] + \int \left[\frac{\epsilon(\vec{r})}{8\pi} |\nabla V(\vec{r})|^2 + \rho_t(\vec{r}) V(\vec{r})\right] d\vec{r}, \tag{3.11}$$

where $V(\vec{r})$ is the total electrostatic potential, Coulomb and electron-ion potential, and $\rho_t(\vec{r})$ is the total charge density.

From the energy functional in equation (3.11), the Poisson equation is obtained using the variational principle $\frac{\delta E}{\delta V} = 0$ [46] , i.e.

$$\frac{\delta \left\{ T_s[\rho_e] + E_{ex}[\rho_e] + \int \left[\frac{\epsilon(\vec{r})}{8\pi} |\nabla V(\vec{r})|^2 + \rho_t(\vec{r}) V(\vec{r})\right] d\vec{r} \right\}}{\delta V} = 0. \tag{3.12}$$

This gives

$$\frac{2}{8\pi} \nabla \cdot \left[\epsilon(\vec{r}) \nabla\right] V(\vec{r}) + \rho_t(\vec{r}) = 0, \tag{3.13}$$

and finally the Poisson equation,

$$\nabla \cdot [\epsilon(\vec{r})\nabla]\, V(\vec{r}) = -4\pi\rho_t(\vec{r}). \tag{3.14}$$

The electronic charge density, $\rho_e(\vec{r})$ may be obtained using density functional theory, where $\rho_n(\vec{r})$ and $\rho_c(\vec{r})$ are known (externally) [46]. Using the Poisson equation, in equation (3.14), one may obtain the electrostatic potential $V(\vec{r})$.

Let me emphasize again that the total charge density $\rho_t(\vec{r})$ does not only have electronic and nuclear charges, but also external charges. These external charges lead to a classic charge density $\rho_c(\vec{r})$, which ensures that charge neutrality is satisfied. This means that,

$$\int_{\Upsilon} \rho_t(\vec{r}) d(\vec{r}) = 0, \tag{3.15}$$

where Υ is the region with the ESM.

We can formally define a Green's function related to the Poisson equation (3.14) [46],

$$\nabla \cdot [\epsilon(\vec{r})\nabla]\, G(\vec{r}, \vec{r'}) = -4\pi\delta(\vec{r} - \vec{r'}). \tag{3.16}$$

We may then obtain the solution of the Poisson equation for appropriate boundary conditions. These boundary conditions must be imposed on equation (3.14) and also on equation (3.16), as the electrostatic potential $V(\vec{r})$ follows from,

$$V(\vec{r}) = \int G(\vec{r}, \vec{r'})\rho_t(\vec{r'}) d\vec{r'}. \tag{3.17}$$

The Green's function itself may be determined analytically for specific boundary conditions, and then we obtain the electrostatic potential $V(\vec{r})$ for the system from the knowledge of $\rho_t(\vec{r})$.

Assume that, $\epsilon(\vec{r})$ only depends on the z-direction, and that the periodicity in the slab is retained parallel to the surface. Then for vectors $\vec{r}_{||}$, $\vec{r'}_{||}$ parallel to the surface, equation (3.16) becomes,

$$\left\{\partial_z \left[\epsilon(z)\partial_z\right] + \epsilon(z)\nabla_{||}^2\right\} G\left(\vec{r}_{||} - \vec{r'}_{||}, z, z'\right) = -4\pi\delta\left(\vec{r}_{||} - \vec{r'}_{||}\right)\delta\left(z - z'\right) \tag{3.18}$$

In the Laue representation [46], equation (3.18) becomes

$$\left\{\partial_z \left[\epsilon(z)\partial_z\right] + \epsilon(z)g_{||}^2\right\} G\left(\vec{g}_{||}, z, z'\right) = -4\pi\delta\left(z - z'\right) \tag{3.19}$$

Where $g_{||} = |\vec{g}_{||}|$, is the absolute value of a reciprocal lattice vector that is parallel to the surface.

Imposing the following boundary conditions to equation (3.14) and/or (3.18) will specify a number of useful Green's functions [46].

(i) pbc: Here the system preserves the periodicity of the system, no ESM is applied to the system.

(ii) bc1: $\partial_z V(\vec{g}_{||}, z)|_{z=\pm\infty} = 0$, $\epsilon(z) = 1$ everywhere.

Here the ESM in medium I and II is vacuum. This is known as open boundary conditions. In this case no screening takes place. The configuration is $vacuum - slab - vacuum$.

(iii) bc2: $V(\vec{g}_{||}, \pm z_1) = 0$, $\epsilon(z) = \begin{cases} \infty, & \text{in medium I.} \\ \infty, & \text{in medium II.} \\ 1, & \text{in the region between the two media.} \end{cases}$

Here the configuration is $metal - slab - metal$.

(iv) bc3: $\begin{cases} V(\vec{g}_{||}, z)|_{z=z_1} = 0, \\ \partial_z V(\vec{g}_{||}, z)|_{z=-\infty} = 0 \end{cases}$, $\epsilon(z) = \begin{cases} 1, & \text{in medium II.} \\ \infty, & \text{in medium I.} \end{cases}$

Here the configuration is $metal - slab - vacuum$.

(v) $\partial_z V(\vec{g}_{||}, z)|_{z=\pm\infty} = 0$, $\epsilon(z) = \begin{cases} \epsilon_r, & \text{in medium I and II.} \\ 1, & \text{between the two media.} \end{cases}$

Here the slab is sandwiched between two media with finite dielectric constant, ϵ_r, the configuration is $medium - slab - medium$. The dielectric constants, $\epsilon = 1$ and $\epsilon = \infty$ are for vacuum and metal respectively.

For example, by solving equation (3.19) with boundary condition (ii), the Green's function [46] is,

$$G\left(\vec{g}_{||}, z, z'\right) = \frac{4\pi}{2g_{||}} \exp\left(-g_{||}|z - z'|\right) \tag{3.20}$$

Substituting equation (3.20) back into equation (3.17), we obtain the electrostatic potential of the system. This boundary condition applies to neutral systems. Otherwise for $g_{||} = 0$, $\partial_z V(0, -\infty)$ should not be zero. The same applies to $g_{||} = 0$, $\partial_z V(0, +\infty)$ should not be zero.

In this work boundary condition (iv) is often used. With this boundary condition one can introduce excess charges into the system. The metal will induce an equal and opposite image charge to neutralize the overall system. This provides screening of the charges to prevent energy divergence.

3.4 Quantum Espresso

Quantum Espresso [45] is a program package put together to model materials, and to calculate their electronic structure. The code is based on density functional theory, plane wave basis sets and pseudopotentials for representation of the ionic cores. The code allows one to use different exchange-correlation functionals. It also has an ESM option, which makes it possible to study charged materials, and particularly non-periodic or partially periodic systems like a double layer (which is not periodic in the z-direction). With this code I will obtain the total energies, potential energies and charge densities of a double-layer system to finally calculate its capacitance.

Chapter 4

Results and discussion

Our set-up to determine double layer capacitances will consist of an electrode, a liquid and ions solvated by the liquid. There are many different approaches to study a charged system using ab initio methods. In one study Neurock and Filhol [49] performed calculations of a charged electrode. They charged the electrode by addition and subtraction of electrons from the electrode. And they also introduced an oppositely charged background charge(jellium) to neutralize the system. The disadvantage of this approach is that the oppositely charged ions from the jellium are distributed everywhere in space. This makes the potential outside the surface of the electrode very small. Another approach is called the effective screening medium (ESM). It was originally suggested by Sugino and Otani [46]. Their method allows one to study charged metal-liquid interfaces as well, which was discussed in section 3.3 of this dissertation. Their approach will be used throughout this work.

For all calculations done in this work, Quantum Espresso [45] is used. Preliminary studies are done first in this chapter to study how the system behaves under the influence of the ESM. Then a double layer model is developed for some systems of interest. From these model systems we used different approaches to determine capacitance, and then discuss the results.

4.1 Preliminary results

The system that is studied in this section is periodic in two dimensions. It consists of 27 aluminium atoms, 32 water molecules and a sodium ion. The aluminium atoms form the electrode, with three layers of 9 atoms per layer per unit cell. The layers are arranged such that only the first layer is in contact with the electrolyte. The water molecules and the sodium ion are a model electrolyte, where water surrounds the ions to shield them from strong

fields that arise during the formation of a double layer.

Different simulations were done with different boundary conditions for the ESM. First we only considered an electrode with the boundary condition described as bc1 (see section 3.3), which specifies both ESM media as vacua. The results are shown in Figure 4.1. From the figure, one can see that the potential is flat on both sides of the cell, as this system was not charged. The boundary condition bc1 does not allow charges to be introduced into the system, and the system has open boundaries. Across a vacuum the potential is constant, and therefore the flat potential away from the slab shows that there is vacuum. The charge density is located around the aluminium layers, and decays into vacuum on both sides of the slab.

Then we considered a full system under different boundary conditions. This time we charged the system, and in order to prevent energy divergence we used bc3. This boundary condition allows excess charge to be introduced into the system, and the metal ESM screens the charges to prevent energy divergence. In Figure 4.2, the black curve, labelled pbc, is the result for a reference system, where we retained the full periodicity of the system. The red curve, labelled bc3, is for a charged system with boundary condition bc3. The three dips in the potential show the positions of the aluminium atoms in their respective layers. Around $z = 2$ Å is the surface of the electrode. Beyond the surface of the electrode there is water.

The vacuum ESM medium labelled **ESM1** in Figure 4.2a, is located to the left of the electrode as seen in Figure 4.2a. There, the potential is not flat for both curves. This is due to the fact that we did not allow for sufficient vacuum regions before the electrode. Sufficient vacuum is needed to shield the vacuum ESM from the charges on the electrode so that there is no potential difference in the vacuum ESM. For the charged system, one can observe a dipole potential, which leads to a little dip in the curve around $z = -11$ Å at **ESM1**. It is caused by the dipole layer at the interface between the electrode and the vacuum as expected from the classical boundary conditions of electrodynamics [50]. Another dipole layer is observed near the **ESM2** (metal), which is located to the right of the water molecules.

On the electron density plot, Figure 4.2b, there is no difference between the two systems. This is due to the equal number of atoms in both systems. The plot does not drop to zero at both edges of the cell, which is due to insufficient vacuum before the electrode.

The configuration used in Figure 4.3 is different from the configuration used in Figure 4.2. Figure 4.3, shows the total electrostatic potential and charge density of two different systems. One system is labelled AlH_2O, because it contains no sodium ion. The other system labelled AlH_2ONa, which contains sodium. The two systems have an electrolyte that is positively

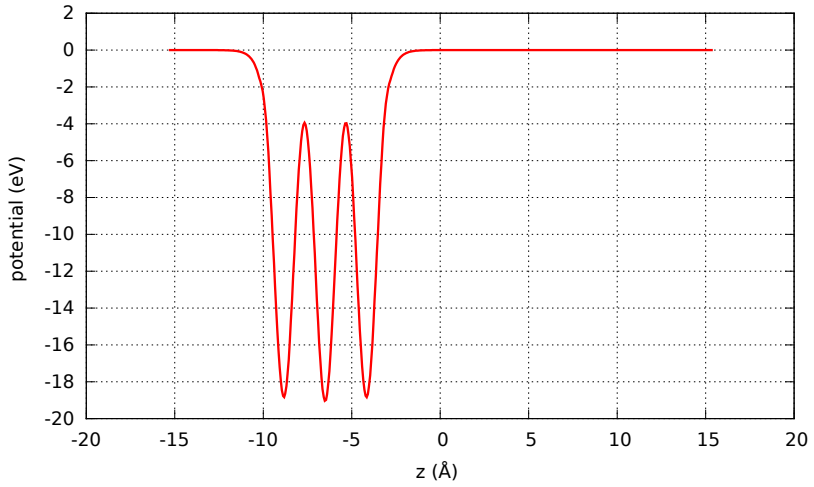

(a)

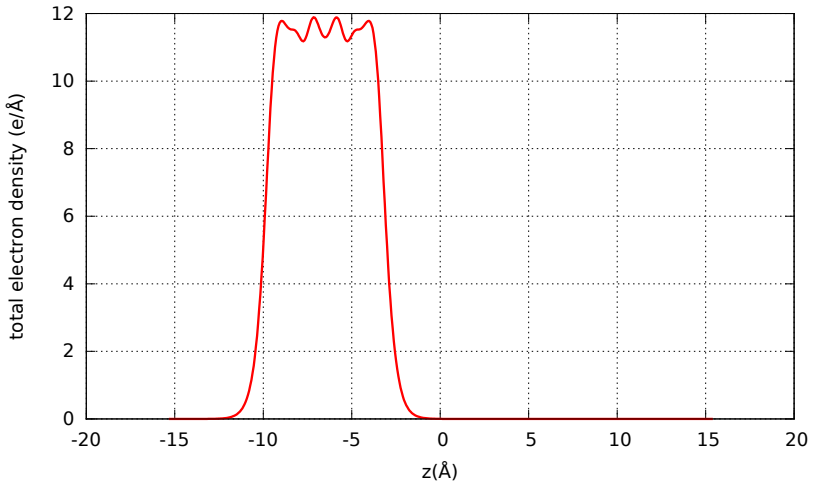

(b)

Figure 4.1: The plot of potential (a) and electron density (b), as a function of the distance from the surface (z-plane) of the electrode for a system of 27 aluminium atoms. The boundary condition is bc1, and the system is not charged.

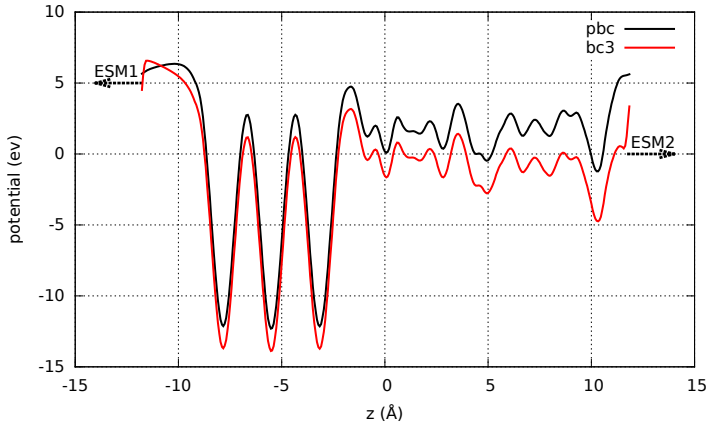

(a)

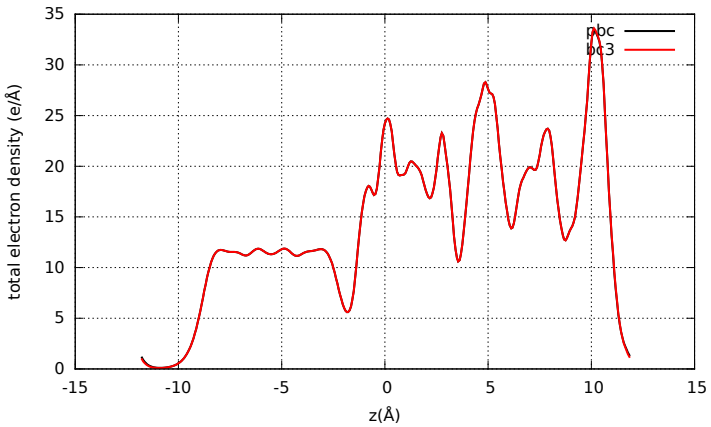

(b)

Figure 4.2: The graphs of the potential (a) and the electron density (b) for the system AlH_2ONa, when there is insufficient vacuum between the electrode and the ESM medium. **ESM1** represents vacuum and **ESM2** represents a metal. The red curve(labelled bc3) is for the charged system. The black curve (labelled pbc) is a reference system where the periodicity of the system is preserved. For pbc the system is not charged and for bc3 the system is charged.

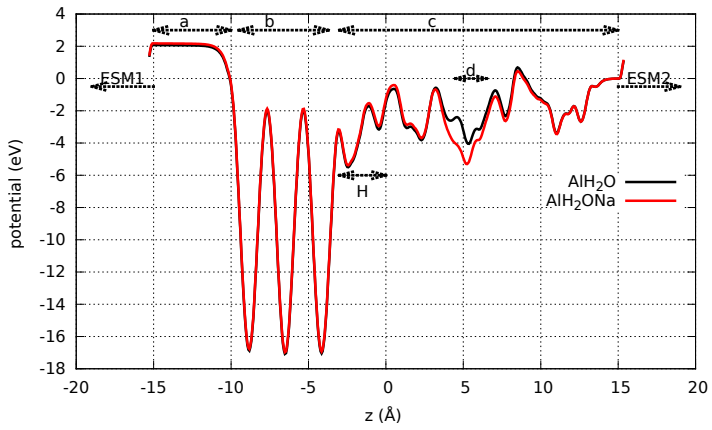

(a)

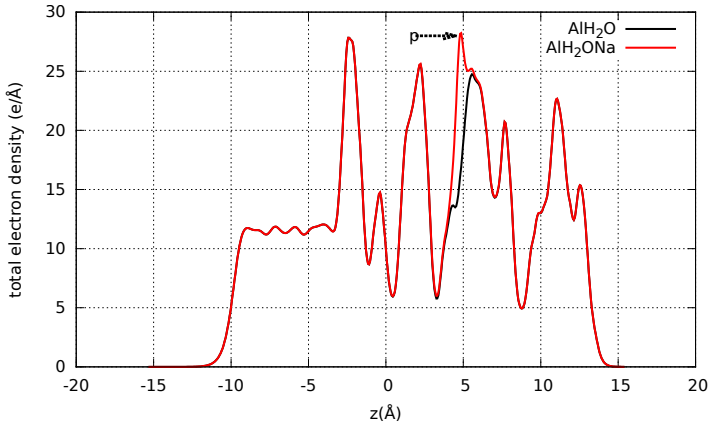

(b)

Figure 4.3: Plot (a) is the potential and (b) electron density for systems AlH_2ONa and AlH_2O. Shifted position of the atoms in the z-plane to give more vacuum left of the electrode. In (a), the region **a** is the vacuum, **b** is the electrode, **c** is the electrolyte with water molecules, **d** is where Sodium is positioned, **H** is the Helmholtz layer, **ESM1** (vacuum) and **ESM2** (metal). And in (b), **p** is the peak that shows the gain of electron when sodium is introduced in the system. Both systems are charged.

charged and there is enough space for a vacuum slab, marked **a** in Figure 4.3a. We can see this from the flattened potential before the electrode, where **ESM1** is vacuum. The potential in this medium is used as energy reference for the system since it is constant. **ESM2** is the ESM medium that represents a metal. It screens the charges introduced into the system. The sodium ion is placed at $z = 4.7$ Å, marked d in Figure 4.3a. This gives the distance between the sodium ion and the surface of the electrode to be 9 Å. When the sodium ion is introduced, there is a significant change in potential and charge density at the location where the sodium ion is placed. In the charge density plot, Figure 4.3b, the introduction of the sodium is seen by a maximum peak, labelled **p**, compared to the system without sodium. It shows a gain in charge density. The region marked as **H** in Figure 4.3a is where the hydrated ions on the electrolyte are adsorbed near the surface of the electrode. This region **H** is called the Helmholtz layer and it gives rise to the double layer capacitance. The distance between the hydrated ions and the surface of the electrode was determined to be around 2 Å [51]. From the double layer theory in chapter 1 of this dissertation, the double layer capacitance is defined by the potential difference and the electrode surface charge density, equation (1.30). The potential in this region includes the dipole potential of the water molecules shielding the sodium ions. It also includes potential from the charges, as in this region there are oppositely charged ions from the surface of the electrode and from the electrolyte.

4.2 Simulation of double layers

The model system consists of a slab, which is sandwiched between two ESM media and is periodic in the x and y-direction. The slab comprises of the electrode and the electrolyte. The electrode has three layers of Pt(111) in the z-direction, each layer has 9 platinum atoms, and the first layer is in contact with electrolyte. Note: in Figure 3.3 the x-direction is used instead of the z-direction. The electrolyte consist of the sodium ion (Na^+) and 32 water molecules, so the overall system is PtH_2ONa. The length of our simulation cell was 32 Å with vacuum of about 4 Å on both sides of the cell before the ESM, and the height was 8.32 Å. For the electrolyte to give correct density, we allowed 15 Å of the length for the electrolyte.

The solvated sodium ion gives rise to a double layer on the surface of the electrode after adsorption. The sodium ions are surrounded by a solvation shell from the water molecules, and electrostatic forces hold the ions in place.

The configuration adopted for this simulation is $metal - slab - vacuum$, as described in section 3.3. The vacuum is on the Pt side of the slab with

$\epsilon = 1$, and the metallic medium of the ESM is placed to the right of the electrolyte side with $\epsilon = \infty$. The interface between the charged surface of the electrode and the solvated ions of the electrolyte is a standard model often used to describe double-layer capacitance [51, 52, 53]. For all calculations the k-points were set to $(3 \times 3 \times 1)$ on the Monkhorst-Pack grid, as shown in Figure 3.2. The positions of the electrode atoms were converged since they are placed in a fixed position, only the water molecules and the sodium ions are placed randomly. We relaxed the water molecules and the sodium ion using the GPAW [54] code with the exchange correlation functional PBE [55]. And the plane wave cut-off energy and the charge density cut-off were set to 60 Ry and 600 Ry, respectively. We used the exchange correlation functional PBE [55]. In this work we generated 8 configurations with different positions of Na^+.

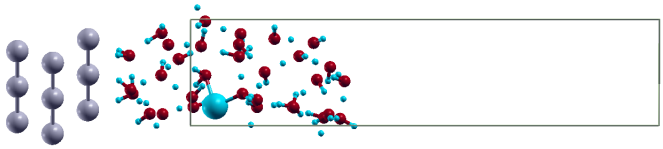

Figure 4.4: Snapshot of the arrangement of atoms in one of the configurations for PtH_2ONa, silver = Pt, red = Oxygen, small blue = Hydrogen, big blue = Sodium.

Within the slab the number of atoms is held fixed throughout our calculations. The water molecules shield the ions of the electrolyte from the fields created during the formation of a double layer near the surface of the electrode.

It has been shown before that it is possible to study charged water/metal systems from a first principles approach [51], and in particular the water/Pt(111) interface has been studied using these methods [56].

4.2.1 Charge on the system

By charging the system we essentially bring a test charge from infinity to a specific point P along the z-axis, which results in a potential difference.

The system consist of two phases, which are the metal electrode and the electrolyte. They form a double layer system when charge is introduced

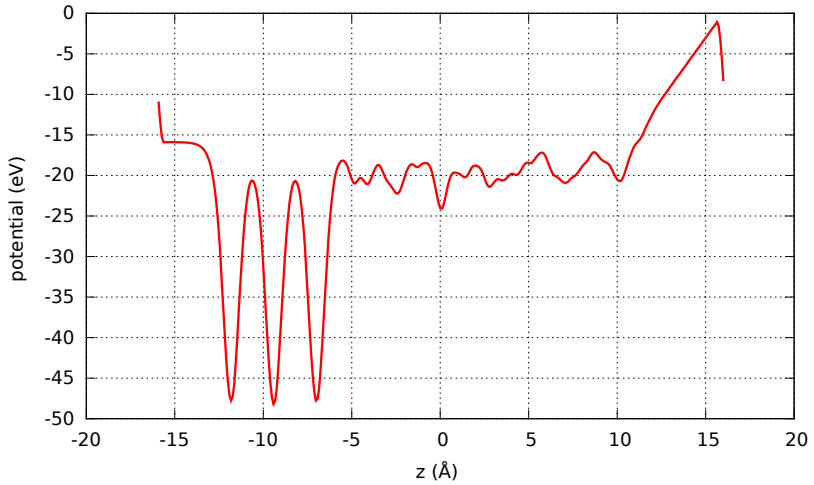

(a)

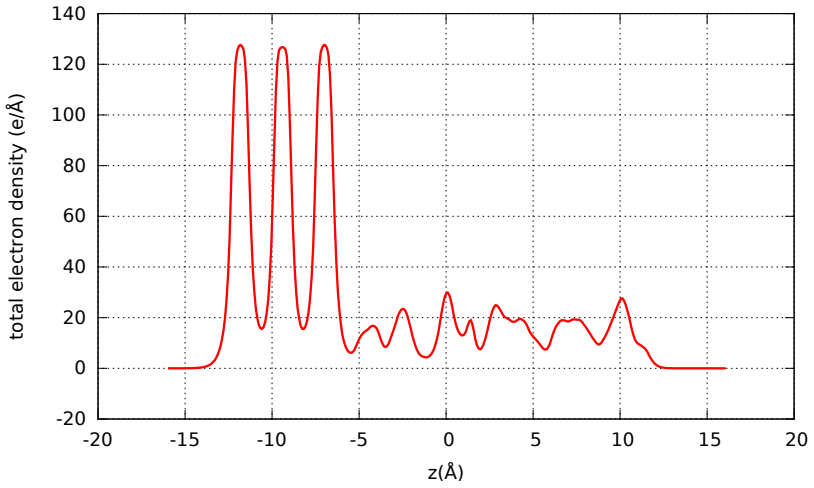

(b)

Figure 4.5: Plot for one configuration, (a) is the potential of the system and (b) is the charge density of the system, the system is PtH_2ONa (charged).

into the system, which happens near the surface of the electrode. The total potential across the interface is the sum of the classical potentials due to the positive and negative charges and the potential due to the orientation of dipoles related to the water molecules. It is given by,

$$V = \text{electrostatic potential} + \text{dipole potential} \tag{4.1}$$

And the total potential difference across the electrode-electrolyte interface results from the sum of the differences for each of the two contributions. This gives,

$$\Delta V = \Delta\,(\text{electrostatic potential}) + \Delta\,(\text{dipole potential}) \tag{4.2}$$

I will discuss the electrostatic potential first, and then I will discuss the dipole potential.

4.2.2 Electrostatic potential

The overall electrostatic potential is denoted by ϕ. For the electrode-electrolyte interface, we now want to describe several components separately.

Electrode:

The potential that we encounter by bringing a test charge from infinity to a point P outside the surface of the electrode. We thus charge a region, which is just outside the surface of the electrode, because the relevant electrons do not sit directly on the surface of the electrode. This potential near the surface of the electrode, is referred as the outside electrode potential ϕ_M.

Electrolyte:

The electrolyte is charged due to the Na^+ ion, leading to a potential outside the surface of the electrolyte, which is called the outer electrolyte potential ϕ_S.

Next we combine the two systems to obtain a charged model system, PtH_2ONa (charged). This system forms a double-layer, and in order to get the potential across the electrode-electrolyte interface, we have to take the difference between ϕ_M and ϕ_S to get,

$$\Delta\phi = \phi_M - \phi_S. \tag{4.3}$$

This potential difference is solely due to the charges in the system, and therefore it is a difference in electrostatic potential. It is also referred to as the contact potential difference or the Volta potential difference. It is discussed in many textbooks of electrochemistry [32, 33]

4.2.3 Dipole potential

The dipole potential, χ , is caused by the dipole orientation of the water molecules, after a charge is introduced. The full dynamics of their orientation is beyond the scope of this work, we are only interested in averaging over some variations of the potential. To visualise the dipole potential we again analyse various contributions separately.

Electrode:

The electrode has a very small dipole potential, which can be neglected, such that $\chi_M = 0$. In this case we do not have excess charges resulting in double-layer formation. This mean that the surface of the electrode is neutral Pt(neutral), only the electrolyte is charged.

Electrolyte:

Here again, we start with a test charge at infinity, and bring it to a point P in the electrolyte. Point P is just inside the surface of the dipole layer. Technically speaking we thus charge the electrolyte phase, i.e H_2ONa (charged). This will generate a potential across the surface of the electrolyte χ_S. This potential on the surface of the electrolyte is only due to the orientation dipole in the dipole layers after charging the phase.

The dipole potential difference is given by

$$\Delta\chi = \chi_M - \chi_S. \tag{4.4}$$

Since $\chi_M = 0$, then we have

$$\Delta\chi = -\chi_S. \tag{4.5}$$

Now from equation (4.1) we get the total potential across the interface,

$$V = \phi + \chi. \tag{4.6}$$

From equation (4.2), we will get the total potential difference,

$$\begin{aligned} \Delta V =& \Delta\phi + \Delta\chi & (4.7)\\ =& (\phi_M - \phi_S) + (-\chi_S)\,. & (4.8) \end{aligned}$$

In general we find that,

$$\begin{aligned} \Delta V =& (\phi_M - \phi_S) + (\chi_M - \chi_S) & (4.9)\\ =& (\phi_M + \chi_M) - (\phi_S + \chi_S) & (4.10)\\ =& V_M - V_S. & (4.11) \end{aligned}$$

Equation (4.11) is the total potential difference on the electrode-electrolyte interface, where

$$V_M \equiv V^{charged}_{PtH_2ONa}, \tag{4.12}$$

is the potential for the whole system.
On the other hand the term

$$V_S \equiv V^{charged}_{H_2ONa} + V^{neutral}_{Pt}, \tag{4.13}$$

includes the potential from the electrolyte and the electrode.
This gives,

$$\Delta V = V^{charged}_{PtH_2ONa} - \left(V^{charged}_{H_2ONa} + V^{neutral}_{Pt}\right). \tag{4.14}$$

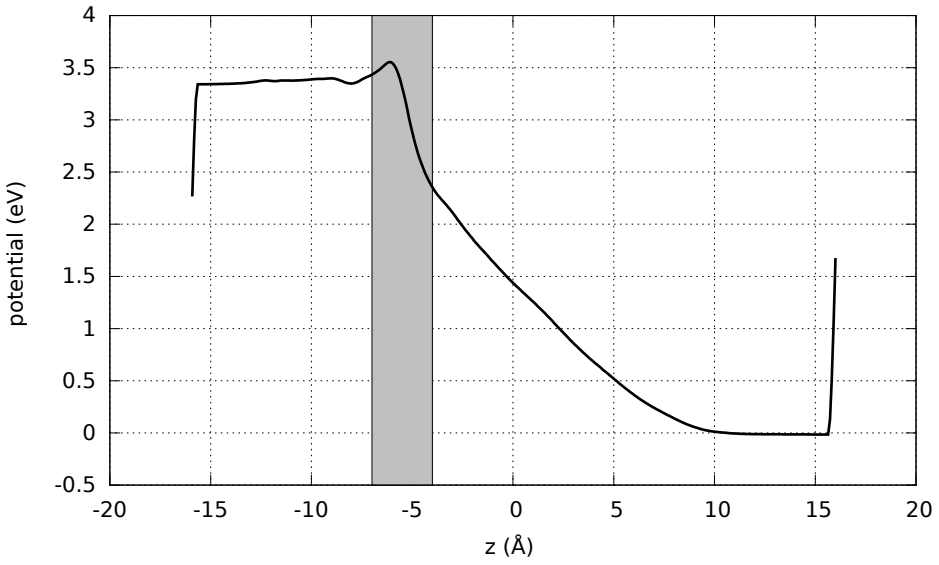

Figure 4.6: Graph of average total potential difference (ΔV) on the electrode-electrolyte interface. The gray shaded part is the Helmholtz layer which is estimated to be around 3 Å wide, its potential difference will be written as ΔV_H.

The potential is averaged in the x and y-direction and plotted along the z-direction. The value for the total potential difference in the Helmholtz layer in Figure 4.6 is

$$\Delta V_H = 1.08 \pm 0.13 \text{ eV} \tag{4.15}$$

This computation was done for different configurations of the system; in each configuration the water molecules has different orientations and the

sodium ion has different position within the electrolyte. There is an uncertainty in the results, as there are systematic errors in the numerics caused by the introduction of the ESM. Furthermore our calculations comprise only a half cell, and other errors also affect the final results. These errors include the screening potential that arises when the ESM screens the ions of the electrolyte solution. There are techniques to overcome such errors [57, 58], but in this work I used Quantum Espresso [45] which is the tool that was available and accessible, which does not compensate for these errors.

4.2.4 Charge density

For the charge density, we follow the same procedures that we developed for the total potential difference. The total charge density is defined as the difference between the charge density of the complete charged system and the sum of the charge densities of the electrolyte and neutral electrode,

$$\Delta\rho_z = \rho^{charged}_{PtH_2ONa} - \left(\rho^{charged}_{H_2ONa} + \rho^{neutral}_{Pt}\right). \tag{4.16}$$

The charge density is again averaged in the x and y-direction and plotted along the z-direction. Figure 4.5b shows the charge distribution of the system. The positive values indicate electron density accumulation and the negative values indicate electron density depletion.

From Figure 4.7, one can observe that near the surface of the electrode the charge accumulation is at its maximum. As one moves away from the surface $\Delta\rho$ becomes zero, which shows that the system becomes neutral. The region between -10 Å and -5 Å is the location of the electrode. In this region we observe both a gain and a loss of charge.

The total charge Q_z, is calculated by integrating the charge density over the electrode/electrolyte interface along the z-direction [59]. It is given by

$$Q_z = \int_{z_{min}}^{z_{max}} \Delta\rho(z')dz'. \tag{4.17}$$

Here z_{max} is the point of the electrode/electrolyte interface, and z_{min} is a point in the z-direction where electron density difference has vanished to zero. This factor quantifies the electron transfer in the system, which is calculated to be

$$Q_z = 0.30 \pm 0.02\text{e}, \tag{4.18}$$

where $\text{e} = 1.602 \times 10^{-19}$ C.

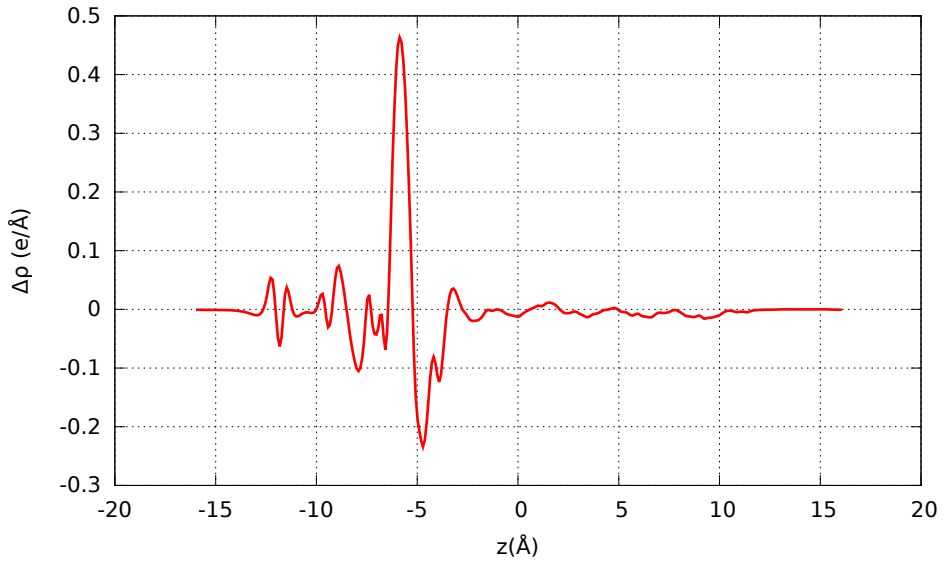

Figure 4.7: Graph of the total charge density difference of the system, the system is PtH_2ONa(charged).

4.3 Capacitance

Now I will study the capacitance of the system in two different approaches, from the potential difference and total energy of the system.

4.3.1 Capacitance from potential difference:

In this approach I will compare calculated capacitance using the Helmholtz potential difference ΔV_H, and the total potential difference ΔV of the system from Figure 4.6.

To calculate the capacitance of the system based on the Helmholtz potential difference ΔV_H, I need the surface charge density σ. The electrode consists of 3 layers of platinum(111), and the calculated surface area of the electrode is,

A = 59.9 Å^2 .

This gives a surface charge density of,

$$\sigma = \frac{Q}{A} = \frac{4.81 \times 10^{-20}\ \text{C}}{59.9 \times 10^{-16}\ \text{cm}^2} = 0.80 \pm 0.06 \times 10^{-5}\ \text{C} \cdot \text{cm}^{-2}. \qquad (4.19)$$

Previously determined charge densities for platinum electrode are 1.19×10^{-5} C $\cdot$ cm^{-2} [58] and 1.14×10^{-5} C $\cdot$ cm^{-2} [60]. These values were obtained using ab initio

methods, their surface charge density values are comparable to the calculated surface charge density given in equation (4.19). The difference comes from the surface area of the electrode used.

From this value of surface charge density, I have calculated the capacitance of the system per area of the electrode, i.e.

$$\frac{C}{A} = \frac{\sigma}{\Delta V_H} \tag{4.20}$$

$$= \frac{0.80 \times 10^{-5}\ \mathrm{C \cdot cm^{-2}}}{1.08\ \mathrm{V}} = 7.41 \pm 0.96 \times 10^{-6}\ \mathrm{F \cdot cm^{-2}}. \tag{4.21}$$

This capacitance is also called the Helmholtz capacitance [61], which was discussed in equation (1.31). It does not depend on the electrolyte concentration, it only depends on the surface area of the electrode where the charge is stored.

We also calculated the capacitance from the total potential difference ΔV of the system as seen in Figure 4.6, the total potential difference $\Delta V = 3.4 \pm 0.26$ eV. To calculate the surface charge density we use the value of the elementary charge $Q_e = 1.602 \times 10^{-19}$ C, to get the surface charge density $2.67 \times 10^{-5}\ \mathrm{C \cdot cm^{-2}}$.

Using these values, we calculate the capacitance $7.85 \pm 0.65 \times 10^{-6}\ \mathrm{F \cdot cm^{-2}}$ from the total potential difference ΔV.

The above calculated values for capacitance are comparable using the methods mentioned above. The double-layer capacitance for the carbon electrode has been determined before and it is between 5 $\mu\mathrm{F \cdot cm^{-2}}$ and 20 $\mu\mathrm{F \cdot cm^{-2}}$ [20]. And using the platinum electrode the double-layer capacitance was calculated to be 11×10^{-6} $\mu\mathrm{F \cdot cm^{-2}}$ [60], so our calculated capacitance is within the range.

Differentiating the surface charge density with respect to a change in potential would give the differential capacitance [62, 63, 64],

$$C_d = \frac{\partial \sigma}{\partial \Delta V}. \tag{4.22}$$

We did not study the differential capacitance across the interface. Note that the capacitance from the potential difference was calculated by averaging the electrostatic potential and the charge density for different configurations. I averaged over 8 different configurations of the system retaining the same number of atoms. Throughout the different configurations the position of the atoms in the electrode were kept fixed. The averaging was done since the sodium was not fixed in one specific position. The average position of the sodium away from the electrode surface was about 1.26 Å. The water

dipole also had to be averaged since the orientation of water molecules is not the same in all configurations. Table 5.1 and 5.2 in Appendix (ii) has the Helmholtz potential difference ΔV_H and total potential difference ΔV for each configuration with different position of Na^+, and their respective calculated capacitances. Figure 4.4, shows a snapshot of a single configuration of the system. In this figure one can observe the orientation of the water molecules. However we could not study the dynamics of the dipole orientation of the water molecules, and also not the adsorption of the hydrated ions on the surface of the electrode as in [65, 66]. It would have been an excessive numerical effort for very little gain in accuracy at the moment.

4.3.2 Capacitance from total energy difference:

An alternative method to calculate the capacitance is to use the total energy of the system. Capacitance C is assumed to be related to the change in total energy ΔE as,

$$C = \frac{Q_e^2}{2|\Delta E|}. \tag{4.23}$$

Here, $\Delta E = E^{charged}_{PtH_2ONa} - \left(E^{charged}_{H_2ONa} + E^{neutral}_{Pt}\right)$ and $Q_e = 1.602 \times 10^{-19}$ C is the elementary charge. The energy difference is taken for the same systems for which I worked out the potential difference before.

The calculated total energy difference is,

$$|\Delta E| = 0.17 \pm 0.04 \text{ Ry} = 3.71 \times 10^{-19} \text{ J}. \tag{4.24}$$

This energy difference was averaged over 8 different configurations of the system. The position of the sodium in each configuration was different, as seen in Table 5.3 in Appendix (ii). Also the dipole orientation of the water molecules was not the same in all configurations. This way we tried to include the dynamics of the electrolyte, simply by averaging through different configurations of the system.

With the total energy difference value, we obtain the capacitance of the system as:

$$C = \frac{Q_e^2}{2|\Delta E|} \tag{4.25}$$

$$= \frac{(1.602 \times 10^{-19} \text{ C})^2}{2\,(3.71 \times 10^{-19} \text{ J})} = 3.46 \times 10^{-20} \text{ F}. \tag{4.26}$$

Table 4.1: Double layer capacitance from different electrode materials.

Electrode	Electrolyte	Method of study	Capacitance ($\mathrm{F \cdot cm^{-2}}$)
MoS_2	H_2SO_4	[a]Experiment	70×10^{-3}
Gold	H_2SO_4	[b]Experiment	10×10^{-6}
Graphene	[BMIM][BF_4]	[c]DFT	8×10^{-6}
Pt(111)	Na^+	[d]DFT	11×10^{-6}
Al	LiCl	[e]DFT	10.4×10^{-6}

[a]Reference[67] , [b]Reference[68], [c]Reference[69], [d]Reference[60], [e]Reference[70]

Then taking the capacitance of the system per area of the electrode,

$$\frac{C}{A} = \frac{3.46 \times 10^{-20}\ \mathrm{F}}{59.9 \times 10^{-16}\ \mathrm{cm^2}} = 5.80 \pm 1.81 \times 10^{-6}\ \mathrm{F \cdot cm^{-2}}. \tag{4.27}$$

This capacitance is comparable to the capacitance calculated above using the potential difference approach. Here the difference might come from a charge accumulation that was estimated in the Helmholtz layer in the first approach. This comes from the limited information on how to locate the Helmholtz layer in the double layer theory. We might have over estimated the charge accumulation in the Helmholtz layer which gave us higher capacitance. And we might have under estimated the total potential difference of the system ΔV, which resulted in higher capacitance in the potential difference approach. In these two approaches, the potential difference and energy difference were averaged over 8 different configurations. Table 5.1, 5.2 and 5.3 in Appendix (ii) summarises the results we obtained for each configuration. The averaging was done due to the the different orientations of the water molecules and different position of the sodium ions. By properly defining the charge accumulation on the surface of the electrode and by quantifying the contributions from chemical bonding might improve the value for capacitance that we obtained here.

Table 4.1, shows a list of different capacitances obtained both experimentally and using ab initio methods with different electrodes and electrolytes. The experimental values were obtained at different scan rates of 1 $\mathrm{mV \cdot s^{-1}}$ [67] and 10 $\mathrm{mV \cdot s^{-1}}$ [68] , the electrolyte used is $0.5M$ of H_2SO_4 in both experiments. These experimental values strongly depend on the scan rates; the higher the scan rate, the lower is the capacitance one obtains. The experimental capacitance also contains contributions from charge transfer reactions at the electrode called the Faradaic processes. The capacitance that results from this process is called pseudo-capacitance [11, 71]. This type of capaci-

tance is generally greater than the pure electrochemical capacitance. We can see from this table that materials like MoS_2 are excellent candidates to be used as an electrode for a supercapacitor. In this experiment thin film MoS_2 was used which behaves differently from bulk materials. They will provide very high capacitance, due to their morphology, which gives large surface area for double layer formation [72, 73, 74, 67]. But there is also a considerable contribution from pseudo-capacitance, something that is not fully understood up to now. There are a lot of other materials that can be used as the electrode for the double layer capacitance [68, 69, 60, 70]. Note that for the capacitance in table 4.1 which are obtained using DFT, the authors used the potential difference approach. Our results are comparable to these previous studies.

4.4 Summary and Future work

The scope of this work was to estimate the Helmholtz double layer capacitance using ab initio methods. The formation of the double layer on the surface of the electrode results in formation of a strong electric field. To shield the sodium ions, we used water molecules as solvent, and our model electrolyte consisted of sodium ions and water molecules. We did not study the orientation of the dipole of water molecules solvating the sodium ions. To prevent dissociation when charging the system, we used an effective screening medium(ESM). The ESM is a medium of different dielectric constant located at the edges of the simulation cell. As ESM media we used vacuum($\epsilon = 1$) and metal($\epsilon = \infty$); vacuum is used as energy reference, and the metallic medium ensures the neutrality of the system. We had to charge the system in order to simulate the electrochemical double layer of the system. The effect of the ESM was investigated in detail to get a better understanding of this method on a charged system. The lesson we learned in this study is that, when using the ESM, one always has to provide enough vacuum between the ESM media and the electrode. Generally the scheme has shown its usefulness, in particular for our model system. Our model system consisted of platinum electrode and an electrolyte, where the electrolyte consists of water molecules and sodium ions.

The Helmholtz capacitance was estimated based on two approaches. The first approach took into account the approach of the potential variation on the interface; and the second approach took into account the total energy of the system. The capacitance that we obtained is comparable to previous results using ab initio molecular dynamics methods and experimental results. Our methods can certainly be improved to obtain better capacitance, and to

understand the physical chemical processes that influence the capacitance of a given system.

Future research in this field is very open at the moment. We need better theories that can account for all the chemical and electrochemical processes taking place at the surface of the electrode. These processes include the adsorption of ions and the dynamics of solvent molecules. We also need theories for pseudo-capacitance or quantum capacitance, and ways to obtain them using ab initio methods. None of these subjects has been fully understood or studied rigorously up to now, so the prediction of capacitance is not trivial. The lack of proper theory to predict the double layer capacitance requires one to explicitly state what we are referring to when measuring or calculating double layer capacitance. Since different strategies and approaches to calculate or measure double layer capacitance obviously give different results. We are not sure if the experimental values are correct, or if they just measure something else than what our theory predicts. Recently, researchers have used different experimental techniques such as scanning tunnelling microscopy [75] and scanning electrochemical microscopy [76] to improve the measurement of double layer capacitance. And for the theoretical methods, new computational methods have been developed to study the metal-electrode/liquid-electrolyte interface to predict double layer capacitance. However, these theoretical methods do not fully account for the screening of ions in the electrolyte. Having methods that will fully account for the screening of the ions, might assist in accurately defining the electrochemical double layer in the metal-electrode/liquid-electrolyte interfaces and for other systems as well.

Chapter 5

Appendix

(i)

The following derivation is obtained with the assistance of the electrochemistry textbooks [32, 33].

From equation (1.16) we have,

$$\left(\frac{dV}{dx}\right)^2 = \frac{2kT}{\varepsilon\varepsilon_0}\sum_i n_i\left[\exp\left(-\frac{z_i eV}{kT}\right) - 1\right]. \tag{5.1}$$

To simplify equation (5.1) further, we consider a symmetric electrolyte(1:1 or z:z-electrolyte). This mean that $|z_+| = |z_-| = z$ and $n_+ = n_- = n$. Then we can drop the summation and write equation (5.1) as,

$$\left(\frac{dV}{dx}\right)^2 = \frac{2kTn}{\varepsilon\varepsilon_0}\left[\exp\left(-\frac{zeV}{kT}\right) - 1 + \exp\left(\frac{zeV}{kT}\right) - 1\right]. \tag{5.2}$$

Let $y = \dfrac{zeV}{kT}$, then equation(5.2) is written as

$$\left(\frac{dV}{dx}\right)^2 = \frac{2kTn}{\varepsilon\varepsilon_0}\left[e^{-y} - 1 + e^{y} - 1\right] \tag{5.3}$$

$$= \frac{2kTn}{\varepsilon\varepsilon_0}\left[e^{y} - 2 + e^{-y}\right] \tag{5.4}$$

$$= \frac{2kTn}{\varepsilon\varepsilon_0}\left[e^{y} - 2e^{-\frac{y}{2}}e^{\frac{y}{2}} + e^{-y}\right] \tag{5.5}$$

$$\left(\frac{dV}{dx}\right)^2 = \frac{2kTn}{\varepsilon\varepsilon_0}\left[e^{\frac{y}{2}} - e^{-\frac{y}{2}}\right]^2 \tag{5.6}$$

$$= \frac{2kTn}{\varepsilon\varepsilon_0}\left[2\left(\frac{e^{\frac{y}{2}} - e^{-\frac{y}{2}}}{2}\right)\right]^2 \tag{5.7}$$

Using the hyperbolic sine function, we find that

$$\left(\frac{dV}{dx}\right)^2 = \frac{2kTn}{\varepsilon\varepsilon_0}\left[2\left(\frac{e^{\frac{y}{2}} - e^{-\frac{y}{2}}}{2}\right)\right]^2 \tag{5.8}$$

$$= \frac{2kTn}{\varepsilon\varepsilon_0}\left[2\sinh\left(\frac{y}{2}\right)\right]^2 \tag{5.9}$$

$$= \frac{8kTn}{\varepsilon\varepsilon_0}\sinh^2\left(\frac{y}{2}\right). \tag{5.10}$$

Substituting back, $y = \dfrac{zeV}{kT}$

$$\left(\frac{dV}{dx}\right)^2 = \frac{8kTn}{\varepsilon\varepsilon_0}\sinh^2\left(\frac{zeV}{2kT}\right). \tag{5.11}$$

Taking the square root, we get

$$\frac{dV}{dx} = \pm\sqrt{\frac{8kTn}{\varepsilon\varepsilon_0}}\sinh\left(\frac{zeV}{2kT}\right). \tag{5.12}$$

To decide which square root is taken, we consider a positively charged electrode and negatively charged electrode. For a positively charged electrode, $V > 0$ and $\frac{dV}{dx} < 0$. And for a negatively charged electrode $V < 0$ and $\frac{dV}{dx} > 0$. The square root that describes a system which is studied in this work, turns out to be the positive square root: we negatively charge the electrode, and then equation (5.12) is written as,

$$\frac{dV}{dx} = \sqrt{\frac{8kTn}{\varepsilon\varepsilon_0}}\sinh\left(\frac{zeV}{2kT}\right). \tag{5.13}$$

(ii)

Table 5.1: Table of the Helmholtz potential difference (ΔV_H) for each configuration with respective capacitance, and the position of Na^+ from the surface of the electrode. The average capacitance per area, $\frac{C}{A} = 7.26 \pm 0.96\ \mu F \cdot cm^{-2}$.

Configuration	Na^+ position (Å)	ΔV_H (Ry)	$\frac{C}{A}$ ($\mu F \cdot cm^{-2}$)
1	1.43	1.16	6.52
2	-1.68	0.88	8.05
3	1.70	1.12	7.41
4	1.11	1.11	6.42
4	0.08	1.04	7.08
6	2.34	0.90	9.36
7	2.55	1.25	6.91
8	2.52	1.15	6.99

Table 5.2: Table of total potential difference (ΔV) for each configuration with respective capacitance, and the position of Na^+ from the surface of the electrode. The average capacitance per area, $\frac{C}{A} = 9.60 \pm 0.65\ \mu F \cdot cm^{-2}$.

Configuration	Na^+ position (Å)	ΔV (Ry)	$\frac{C}{A}$ ($\mu F \cdot cm^{-2}$)
1	1.43	2.89	9.24
2	-1.68	3.59	7.44
3	1.70	3.24	8.26
4	1.11	3.20	8.35
4	0.08	3.69	7.24
6	2.34	3.18	8.38
7	2.55	3.53	7.57
8	2.52	3.39	7.87

Table 5.3: Table of total energy difference (ΔE) for each configuration with respective capacitance, and the position of Na^+ from the surface of the electrode. The average capacitance per area, $\frac{C}{A} = 6.38 \pm 1.80\ \mu F \cdot cm^{-2}$.

Configuration	Na^+ position (Å)	$\lvert\Delta E\rvert$ (Ry)	$\frac{C}{A}$ ($\mu F \cdot cm^{-2}$)
1	1.43	0.17	5.66
2	-1.68	0.14	7.26
3	1.70	0.19	5.05
4	1.11	0.19	5.05
4	0.08	0.10	9.46
6	2.34	0.24	4.08
7	2.55	0.12	8.16
8	2.52	0.15	6.38

Bibliography

[1] Testa motors charging. `http://www.teslamotors.com/models-charging`. [online; accessed on 2016-02-24].

[2] Testa model s. `http://www.roperld.com/science/TeslaModelS.htm`. [online; accessed on 2016-02-24].

[3] M.R. Palacin. Recent advances in rechargeable battery materials: a chemist's perspective. *Chemical Society Reviews*, 38(9):2565–2575, 2009.

[4] N. Choi, Z. Chen, S.A. Freunberger, X. Ji, Y. Sun, K. Amine, G. Yushin, L.F. Nazar, J. Cho and P.G. Bruce. Challenges facing lithium batteries and electrical double-layer capacitors. *Angewandte Chemie International Edition*, 51(40):9994–10024, 2012.

[5] Electrochemical double layer. `http://large.stanford.edu/courses/2012/ph240/wang-hu2/`. [online; accessed on 2015-03-19].

[6] M.S. Halper and C.J. Ellenbogen. Supercapacitors: A brief overview. *The MITRE Corporation, McLean, Virginia*, pages 1–34, 2006.

[7] M.A. Guerrero, E. Romero, F. Barrero, M.I. Milanés and E. González. Supercapacitors: Alternative energy storage systems. *Przegląd Elektrotechniczny*, 85(10):188–195, 2009.

[8] A. Burke. Ultracapacitors: why, how, and where is the technology. *Journal of power sources*, 91(1):37–50, 2000.

[9] P. Sharma and T.S. Bhatti. A review on electrochemical double-layer capacitors. *Energy conversion and management*, 51(12):2901–2912, 2010.

[10] A. Chu and P. Braatz. Comparison of commercial supercapacitors and high-power lithium-ion batteries for power-assist applications in hybrid electric vehicles: I. initial characterization. *Journal of power sources*, 112(1):236–246, 2002.

[11] B.E. Conway. *Electrochemical supercapacitors: scientific fundamentals and technological applications*. Springer Science and Business Media, New York, 2013.

[12] Maxwell Application Notes. Peak load shaving in a fuel cell powered industrial servo system. `http://www.maxwell.com/images/documents/an-001_peak_load_shaving.pdf`.

[13] M.F. Hordeski. *Emergency and Backup Power Sources: Preparing for blackouts and brownouts*. The Fairmont Press, Inc., 2005.

[14] Uninterruptible power supply in alaska. `http://www.eia.gov/todayinenergy/detail.cfm?id=6910#tabs_ElecStorage-5`. [online; accessed on 2016-03-18].

[15] Electrochemical double layer capacitance. `http://www.solrayo.com/SolRayo/Ultracapacitors.html`. [online; accessed on 2015-11-09].

[16] N.S. Zhai, Y.Y. Yao, D.L. Zhang and D.G. Xu. Design and optimization for a supercapacitor application system. In *Power System Technology, 2006. PowerCon 2006. International Conference*, pages 1–4. IEEE, 2006.

[17] Q. Deyang and S. Hang. Studies of activated carbons used in double-layer capacitors. *Journal of Power Sources*, 74(1):99–107, 1998.

[18] Q. Deyang. Studies of the activated carbons used in double-layer supercapacitors. *Journal of power sources*, 109(2):403–411, 2002.

[19] O. Barbieri, M. Hahn, A. Herzog and R. Kötz. Capacitance limits of high surface area activated carbons for double layer capacitors. *Carbon*, 43(6):1303–1310, 2005.

[20] P. Simon and A. Burke. Nanostructured carbons: double-layer capacitance and more. *The Electrochemical Society interface*, 17(1):38, 2008.

[21] H.L.F. Von Helmholtz. Studies of electric boundary layers. *Wied. Ann*, 7:337–382, 1879.

[22] Li Li Zhang and X.S. Zhao. Carbon-based materials as supercapacitor electrodes. *Chemical Society Reviews*, 38(9):2520–2531, 2009.

[23] G. Gouy. Constitution of the electric charge at the surface of an electrolyte. *J. Phys*, 9(4):457–467, 1910.

[24] D.L. Chapman. A contribution to the theory of electrocapillarity. *The London, Edinburgh, and Dublin philosophical magazine and journal of science*, 25(148):475–481, 1913.

[25] J.N. Israelachvili. Intermolecular and surface forces. Academic Press, San Diego, third edition, 2011.

[26] R.K. Pathria and P.D. Beale. *Statistical Mechanics*. Elsevier, New York, third edition, 2011.

[27] A.A. Kornyshev. Double-layer in ionic liquids: paradigm change? *The Journal of Physical Chemistry B*, 111(20):5545–5557, 2007.

[28] O. Stern. The theory of the electrolytic double-layer. *Z. Elektrochem*, 30(508):1014–1020, 1924.

[29] J.B. McEwen. *Treatment process selection for particle removal*. American Water Works Association Research Foundation, Denver, third edition, 1998.

[30] J.O'M. Bockris and A.K.N. Reddy. *Modern Electrochemistry: An introduction to an interdisciplinary area*, volume 1. Springer Science and Business Media, New York, 1998.

[31] A.J. Bard and L.R. Faulkner. *Electrochemical methods: Fundamentals and applications*. John Wiley and Sons inc, New York, first edition, 1980.

[32] A.J. Bard, L.R. Faulkner, J. Leddy and C.G. Zoski. *Electrochemical methods: fundamentals and applications*, volume 2. John Wiley Sons, New York, 1980.

[33] J.O'M. Bockris and A.K.N. Reddy. *Modern Electrochemistry 2B: Electrodics in Chemistry, Engineering, Biology and Environmental Science*, volume 2. Springer Science and Business Media, New York, 2001.

[34] T. Ziegler. Approximate density functional theory as a practical tool in molecular energetics and dynamics. *Chemical Reviews*, 91(5):651–667, 1991.

[35] P. Geerlings, F. De Proft and W. Langenaeker. Conceptual density functional theory. *Chemical reviews*, 103(5):1793–1874, 2003.

[36] R.O. Jones and O. Gunnarsson. The density functional formalism, its applications and prospects. *Reviews of Modern Physics*, 61(3):689, 1989.

[37] P. Hohenberg and W. Kohn. Inhomogeneous electron gas. *Physical Review*, 136(3B):B864, 1964.

[38] W. Kohn and L.J. Sham. Self-consistent equations including exchange and correlation effects. *Physical Review*, 140(4A):A1133, 1965.

[39] R.G. Parr and W. Yang. *Density-functional theory of atoms and molecules*. Oxford University Press, Oxford, 1989.

[40] J.P. Perdew and K. Schmidt. Jacob's ladder of density functional approximations for the exchange-correlation energy. In *AIP Conference Proceedings*, pages 1–20. IOP Institute of Physics Publishing, LTD, 2001.

[41] A. Szabo and N.S. Ostlund. Modern quantum chemistry: introduction to advanced electronic structure theory. *Modern quantum chemistry*, 1982.

[42] N.W. Ashcroft and N.D. Mermin. *Solid State Physics*. Harcourt College Publishers, New York, first edition, 1976.

[43] H.J. Monkhorst and J.D. Pack. Special points for brillouin-zone integrations. *Physical Review B*, 13(12):5188, 1976.

[44] G. Kresse and J. Furthmüller. Efficient iterative schemes for ab initio total-energy calculations using a plane-wave basis set. *Physical Review B*, 54(16):11169, 1996.

[45] P. Giannozzi, S. Baroni, N. Bonini, M. Calandra, R. Car, C. Cavazzoni, D. Ceresoli, G.L. Chiarotti, M. Cococcioni, I. Dabo et al. Quantum espresso: a modular and open-source software project for quantum simulations of materials. *Journal of Physics Condensed Matter*, 21(39):395502, 2009.

[46] M. Otani and O. Sugino. First-principles calculations of charged surfaces and interfaces: A plane-wave nonrepeated slab approach. *Physical Review B*, 73(11):115407, 2006.

[47] S. Lany and A. Zunger. Accurate prediction of defect properties in density functional supercell calculations. *Modelling and Simulation in Materials Science and Engineering*, 17(8):084002, 2009.

[48] Effective screening medium. `http://sugino.issp.u-tokyo.ac.jp/esm/index.php?SIESTA%2BESM%20Manual`. [online; accessed on 2015-07-23].

[49] J-S. Filhol and M. Neurock. Elucidation of the electrochemical activation of water over pd by first principles. *Angewandte Chemie International Edition*, 45(3):402–406, 2006.

[50] J.D. Jackson. *Classical electrodynamics*. John Wiley and Sons inc, New York, 1999.

[51] O. Sugino, I. Hamada, M. Otani, Y. Morikawa, T. Ikeshoji and Y. Okamoto. First-principles molecular dynamics simulation of biased electrode/solution interface. *Surface Science*, 601(22):5237–5240, 2007.

[52] C.D. Taylor, S.A. Wasileski, J-S. Filhol and M. Neurock. First principles reaction modeling of the electrochemical interface: Consideration and calculation of a tunable surface potential from atomic and electronic structure. *Physical Review B*, 73(16):165402, 2006.

[53] E. Skúlason, G.S. Karlberg, J. Rossmeisl, T. Bligaard, J. Greeley, H. Jónsson and J.K. Nørskov. Density functional theory calculations for the hydrogen evolution reaction in an electrochemical double layer on the pt (111) electrode. *Physical Chemistry Chemical Physics*, 9(25):3241–3250, 2007.

[54] J. Enkovaara, C. Rostgaard, J.J. Mortensen, J. Chen, M. Dułak, L. Ferrighi, J. Gavnholt, C. Glinsvad, V. Haikola, H.A. Hansen et al. Electronic structure calculations with gpaw: a real-space implementation of the projector augmented-wave method. *Journal of Physics: Condensed Matter*, 22(25):253202, 2010.

[55] J.P. Perdew , K. Burke , M. Ernzerhof. Generalized gradient approximation made simple. *Physical Review Letters*, 77(18):3865, 1996.

[56] M. Otani, I. Hamada, O. Sugino, Y. Morikawa, Y. Okamoto and T. Ikeshoji. Electrode dynamics from first principles. *Journal of the Physical Society of Japan*, 77(2):024802, 2008.

[57] K. Inagaki and Y. Morikawa. Simulation tool for atom technology. `http://ann.phys.sci.osaka-u.ac.jp/CMD/STATE-Senri/state_110829.pdf`. [online; accessed on 2016-04-23].

[58] I. Hamada and Y. Morikawa. Density-functional analysis of hydrogen on pt (111): Electric field, solvent, and coverage effects. *The Journal of Physical Chemistry*, 112(29):10889–10898, 2008.

[59] J.H. Masliyah and S. Bhattacharjee. *Electrokinetic and colloid transport phenomena*. John Wiley and Sons inc, New York, 2006.

[60] Y. Ando, Y. Gohda and S. Tsuneyuki. Ab initio molecular dynamics study of the electric double-layer capacitance at solution-electrode interfaces. In *APS Meeting Abstracts*, volume 1, page 35009, 2012.

[61] C. Brett and M.A. Oliveira. *Electrochemistry: principles, methods, and applications*. Oxford Science Publications, Oxford, 1993.

[62] J.R. Macdonald and Jr C.A. Barlow. Theory of double-layer differential capacitance in electrolytes. *The Journal of Chemical Physics*, 36(11):3062–3080, 1962.

[63] V. Lockett, M. Horne, R. Sedev, T. Rodopoulos and J. Ralston. Differential capacitance of the double layer at the electrode/ionic liquids interface. *Physical Chemistry Chemical Physics*, 12(39):12499–12512, 2010.

[64] D.K. Schroder. *Semiconductor material and device characterization*. John Wiley and Sons, New York, 2006.

[65] H. Ogasawara, B. Brena, D. Nordlund, M. Nyberg, A. Pelmenschikov, L.G.M. Pettersson and A. Nilsson. Structure and bonding of water on pt (111). *Physical Review Letters*, 89(27):276102, 2002.

[66] A. Michaelides and P. Hu. Catalytic water formation on platinum: A first-principles study. *Journal of the American Chemical Society*, 123(18):4235–4242, 2001.

[67] J.M. Soon and K.P. Loh. Electrochemical double-layer capacitance of mos2 nanowall films. *Electrochemical and Solid-State Letters*, 10(11):A250–A254, 2007.

[68] B. Piela and P.K. Wrona. Capacitance of the gold electrode in 0.5m h2so4 solution: ac impedance studies. *Journal of Electroanalytical Chemistry*, 388(1):69–79, 1995.

[69] G. Feng , J. Huang , B.G. Sumpter , V. Meunier , and R. Qiao. A "counter-charge layer in generalized solvents" framework for electrical double layers in neat and hybrid ionic liquid electrolytes. *Physical Chemistry Chemical Physics*, 13(32):14723–14734, 2011.

[70] M. Pounds, S. Tazi, M. Salanne and P.A. Madden. Ion adsorption at a metallic electrode: an ab initio based simulation study. *Journal of Physics: Condensed Matter*, 21(42):424109, 2009.

[71] B.E. Conway, V. Birss and J. Wojtowicz. The role and utilization of pseudocapacitance for energy storage by supercapacitors. *Journal of Power Sources*, 66(1):1–14, 1997.

[72] H. Peelaers and C.G. Van de Walle. Elastic constants and pressure-induced effects in mos2. *The Journal of Physical Chemistry C*, 118(22):12073–12076, 2014.

[73] J.L. Feldman. Elastic constants of 2h-mos2 and 2h-nbse2 extracted from measured dispersion curves and linear compressibilities. *Journal of Physics and Chemistry of Solids*, 37(12):1141–1144, 1976.

[74] Z.M. Wang. *MoS2: Materials, Physics and devices*, volume 21. Springer Science and Business Media, New York, 2013.

[75] T.P. Moffat. Scanning tunneling microscopy studies of metal electrodes. *Electroanalytical Chemistry*, 21:212–316, 1999.

[76] A.J. Bard, F.F. Fan and M.V. Mirkin. Scanning electrochemical microscopy. *Electroanalytical chemistry*, 18:243–373, 1994.